LIBRARY
RESEARCH REPORTS DIVISION
NAVAL POSTGRADUATE SCHOOL
MONTEREY, CALIFORNIA 93940

NPS67-86-002CR

NAVAL POSTGRADUATE SCHOOL

Monterey, California

CONTRACTOR REPORT

A BREAKDOWN SURFACE MODEL FOR THERMAL BACKSCATTERING FROM THE EXHAUST PLUME OF A SPACE-BASED HF LASER

Joseph Falcovitz

June 1986

Approved for public release; distribution unlimited.

Prepared for:

Strategic Defense Initiative Office
Washington, DC 20301-7100

NAVAL POSTGRADUATE SCHOOL
Monterey, California

RADM R. H. Shumaker
Superintendent

D. A. Schrady
Provost

The work reported herein was performed for the Naval Postgraduate School by Dr. Joseph Falcovitz under Contract N62271-84-M-3345. The work presented in this report is in support of "Rarefied Gas Dynamics of Laser Exhaust Plume" sponsored by the Strategic Defense Initiative Office/Directed Energy Office. This is the final report for that contract. The work provides information concerning backscattering to spacecraft from a multispecies laser exhaust plume. The project at the Naval Postgraduate School is under the cognizance of Distinguished Professor A. E. Fuhs who is principal investigator.

Prepared by:

ASSIFIED
Y CLASSIFICATION OF THIS PAGE

18 September 1985

REPORT DOCUMENTATION PAGE

AD-A171 616

PORT SECURITY CLASSIFICATION ASSIFIED	1b RESTRICTIVE MARKINGS NONE
CURITY CLASSIFICATION AUTHORITY	3 DISTRIBUTION/AVAILABILITY OF REPORT Approved for Public Release; Distribution Unlimited
CLASSIFICATION/DOWNGRADING SCHEDULE	
FORMING ORGANIZATION REPORT NUMBER(S) 7-86-002CR	5 MONITORING ORGANIZATION REPORT NUMBER(S) NPS67-86-002CR
AME OF PERFORMING ORGANIZATION PH FALCOVITZ	6b OFFICE SYMBOL (If applicable) 67
	7a NAME OF MONITORING ORGANIZATION NAVAL POSTGRADUATE SCHOOL, CODE 67
DDRESS (City, State, and ZIP Code) earch Contractor al Postgraduate School, Code 67 terey, CA 93943-5100	7b ADDRESS (City, State, and ZIP Code) Department of Aeronautics Monterey, CA 93943-5100
AME OF FUNDING SPONSORING RGANIZATION Strategic Defense itative Office	8b OFFICE SYMBOL (If applicable) SDIO/DEO
	9 PROCUREMENT INSTRUMENT IDENTIFICATION NUMBER DGAM60045
DDRESS (City, State, and ZIP Code) O/DEO hington, DC 20301-7100	10 SOURCE OF FUNDING NUMBERS PROGRAM ELEMENT NO: 9760400.25 PROJECT NO: 00 0801 P6221 TASK NO: WORK UNIT ACCESSION NO:

TITLE (Include Security Classification)
REAKDOWN SURFACE MODEL FOR THERMAL BACKSCATTERING FROM THE EXHAUST PLUME OF A SPACE-BASED LASER

PERSONAL AUTHOR(S)
EPH FALCOVITZ

TYPE OF REPORT	13b TIME COVERED	14 DATE OF REPORT (Year, Month, Day)	15 PAGE COUNT
tractor Report	FROM Sept. 85 TO Dec. 85	June 1986	

SUPPLEMENTARY NOTATION

COSATI CODES		
FIELD	GROUP	SUB-GROUP

18 SUBJECT TERMS (Continue on reverse if necessary and identify by block number)
Laser Exhaust, Spacecraft Contamination, Chemical Laser, Exhaust Plume, Breakdown Surface

ABSTRACT (Continue on reverse if necessary and identify by block number)

The purpose of this report is to present a breakdown surface model for evaluating rmal backscattering flow from the supersonic exhaust plume of a gaseous mixture H, HF, H_2, DF and He. Fluxes of these species are considered separately. The del is carefully analyzed and is shown to overestimate the flux. Actual flux levels the heavy corrosive molecules (HD, DF) have been found to be exceedingly low. It is cluded that the contribution of thermal backscattering to contaminating flux of HF DF can be neglected. This work is an extension and modification of the recent sis work done by S. E. McCarty at the Naval Postgraduate School.

DISTRIBUTION/AVAILABILITY OF ABSTRACT ☒ UNCLASSIFIED/UNLIMITED ☐ SAME AS RPT ☐ DTIC USERS	21 ABSTRACT SECURITY CLASSIFICATION UNCLASSIFIED
NAME OF RESPONSIBLE INDIVIDUAL LEN E. FUHS, Distinguished Professor	22b TELEPHONE (Include Area Code) 408/646-2948 — 22c OFFICE SYMBOL Code 72

FORM 1473, 84 MAR — 83 APR edition may be used until exhausted. All other editions are obsolete

SECURITY CLASSIFICATION OF THIS PAGE

☆ U.S. Government Printing Office: 1986—606-24

ABSTRACT

The purpose of this report is to present a breakdown surface model for evaluating thermal backscattering flux from the supersonic exhaust plume of a space-based HF laser. The plume is of ring symmetry. It consists of a gaseous mixture of H, HF, H_2, DF and He. Fluxes of these species are considered separately. The model is carefully analyzed and is shown to overestimate the flux. Actual flux levels of the heavy corrosive molecules (HF, DF) have been found to be exceedingly low. It is concluded that the contribution of thermal backscattering to contaminating flux of HF and DF can be neglected. This work is an extension and modification of the recent thesis work done by S. E. McCarty at the Naval Postgraduate School.

ACKNOWLEGEMENT

The ideas leading to this work crystalize through numerous discussions with LCDR Scott E. McCarty and Distinguished Professor Allen E. Fuhs. This Contractor report constitutes in fact an extension and generalization of LCDR McCarty's MSAE Thesis. Their help and cooperation are gratefully acknowledged.

TABLE OF CONTENTS

LIST OF FIGURES

1. INTRODUCTION

This report is a presentation of one part of a study on the contaminating backflow from the exhaust plume of a large space-based HF laser (Figure 1). The exhaust plume is an underexpanded supersonic ring-jet, designed to stay clear of the spacecraft by maintaining a Prandtl-Meyer turning angle at the nozzle lips of well below 90°. However, it is well known from experience with rocket plumes in space[1,2] that cavity regions (where continuum gasdynamic theory predicts vacuum) are filled with a free-molecular flow. This back flow is largely due to viscous effects, which give rise to a "spill-over" of the boundary layer around the nozzle lip[3]. Assuming the boundary layer can be eliminated (e.g., an expanding step design of the nozzle lip), there are two more mechanisms which lead to backflow: thermal backscattering and scattering by ambient molecules traveling at orbital speeds. Since these effects are a small perturbation to the exhaust flow field, they can be considered independently (the total backflow will be a superposition of contributions due to these two effects). As a first phase of our broader study, we consider solely the contribution of thermal backscattering to backflow from a ring-plume of an HF laser, via a simple model of molecular effusion from a breakdown surface, fashioned after ideas suggested by Noller[4]. Our results indicate that the backflow of the heavier contaminants (HF, DF) due to thermal backscattering is negligible.

Naturally, our study pertains to presumably typical operating conditions of the HF laser. These operating conditions were largely determined from a report on some HF laser tests conducted at TRW in 1971[5] (in particular, Table 5, Test III, of this report). The typical parameters at the nozzle exit

are:

Composition (mole fractions):	[H] = .091, [HF] = .091, $[H_2]$ = .104, [DF] = .135, [He] = .579
Specific Heats Ratio:	γ = 1.54 (assuming ideal gas)
Mach Number	M_1 = 4.0
Average Molecular Weight	W_A = 7.27 [kg/kg mole] (1.1)
Stagnation Temperature	T_o = 2300 [K]
Stagnation Density	ρ_o = 0.0075 [kg/m^3]
Molecular Diameter, assuming it is uniform for all species (hard-sphere collisions)	D = 2.5 x 10^{-10} [m]

The exit Mach number can be chosen higher than M_1 = 4, but not considerably lower than this value, since M_1 = 4 results in a modest clearance angle of 41° between the limiting (vacuum) characteristic of the lip-centered rarefaction fan and the spacecraft. We assume isentropic flow throughout the diffuser[5], so that upon specifying the composition and flow variables at the diffuser inlet, along with M_1 at the diffuser exit, the exit flow is fully determined. One exception to this definition, however, is the stagnation temperature, which was estimated as T_o = 1400 [K] at the diffuser inlet[5]. We set T_o = 2300 [K], which corresponds to complete hydrogen recombination, even though the flow in the diffuser is of a nearly frozen composition due to the low rate of hydrogen recombination[5]. The reason for this choice is that given the uncertainty in determining T_o, which results from an uncertainty in the degree of hydrogen recombination, it is the most pessimistic choice, resulting in higher thermally backscattered flux.

The model that we propose for evaluating the backscattered flux arriving

at the spacecraft (Figures 1, 2) is based on the effusive breakdown surface concept suggested by Noller[4]. The gradual transition from continuum to collisionless flow, which invariably takes place at the outer fringes of exhaust plumes having a near-vacuum background environment, is replaced by an abrupt change. We assume that the flow regime in each stream tube changes from continuum (with local thermodynnamic equilibrium) to collisionless, upon crossing some breakdown surface.

An important simplification is introduced in the case of a large-radius spacecraft (about 2.5[m]), by observing that the temperature along the breakdown surface decreases so sharply with the distance from the nozzle lip, that the segment contributing significantly to thermal backscattering is only about 0.01 to 0.1[m] long. Consequently, the lip-centered rarefaction ring-fan may well be approximated by the standard (planar) Prandtl-Meyer flow field.

The structure of this report is as follows. The breakdown surface and the molecular effusion flux from it are obtained in closed-form expressions in Section 2. Section 3 is devoted to the spatial integration scheme, which is the evaluation of the flux arriving at a certain point on the spacecraft. Results of flux distribution along the spacecraft for the presumed laser operating range are presented and discussed in Section 4, followed by a critical examination of the breakdown surface model. Conclusions are given in Section 5, and Section 6 is a list of references. The code RINGBD, which computes the flux by numerical integration over the breakdown (effusing) surface, is given in Appendix A.

2. BREAKDOWN SURFACE AND EFFUSION FLUX

Our model for the thermally backscattered flux arriving at the surface of the spacecraft is essentially a modification of Noller's concept of a breakdown effusive surface[4]. We substitute his definition of a breakdown surface by a similar one introduced by Bird[6, Section 8.3]. We obtain the one-sided effusion flux from the breakdown surface by integrating over velocity space as suggested by Noller[4], except for the fact that we compute flux rather than density and we also consider the flux of species having molecular weight different from the average. In the following, each one of these steps is described in some detail, beginning with the breakdown surface.

As mentioned in the introduction, the lip-centered rarefaction fan is approximated by a planar Prandtl-Meyer flow field (Figure 2). The standard expressions for this flow field have Mach number (M) as the independent parameter, thus M varies between $M = M_1$ at the exit and $M \to \infty$ at the limiting (vacuum) characteristic. (Index 1 always refers to exit conditions, i.e., to parameters evaluated at $M = M_1$).

$$\psi(M) = -\zeta(M) + \zeta_1 + \mu_1 + \frac{\pi}{2}$$

$$\zeta(M) = \Gamma^{1/2}\,\mathrm{ARCTAN}\left[\Gamma^{-1/2}\left(M^2-1\right)^{1/2}\right] \qquad \Gamma=\left(\frac{\gamma+1}{\gamma-1}\right)$$

$$\mu(M) = \mathrm{ARCSIN}(M^{-1}) \qquad (2.1)$$

$$\theta(M) = \psi(M) - \mu(M)$$

where ψ is the angle of characteristic lines, and θ is the angle of the velocity vector (or streamline).

Adopting Bird's definition of a breakdown parameter, which was first introduced in conjunction with a spherical source flow[6, Section 8.3] and later was shown to be meaningful also in a Prandtl-Meyer flow[7], we define the breakdown surface as having a constant value of B, where B is given by:

$$B = \frac{U}{\nu} \frac{1}{\rho} \left|\frac{d\rho}{dS}\right| \tag{2.2}$$

Here ρ, U, ν, S are local flow density, speed, collision frequency, and coordinate along streamlines (thus restricting this definition of B to stationary flows). From the geometrical relationships in a Prandtl-Meyer fan (Figure 2) and from (2.1) we get:

$$\frac{d\rho}{dS} = -(1/R)\left(\frac{d\rho}{d\psi}\right) \sin\mu = -\frac{2}{\gamma+1}\left[M^{-1}(M^2-1)^{1/2}\right](\rho/R)$$

$$\rho(M) = \rho_o \left(1 + \frac{\gamma-1}{2} M^2\right)^{-\frac{1}{\gamma-1}} \tag{2.3}$$

Using the expression for collision frequency[6]:

$$\nu_o = 4(\pi/\gamma)^{1/2} \left(N_o D^2 C_o\right) \tag{2.4}$$

where N_o, C_o, D are stagnation number density, stagnation sound speed, molecular diameter, and using U = MC in conjunction with (2.2) and (2.3), we get:

$$R_B(M) = (BN_oD^2)^{-1} \frac{(\gamma/\pi)^{1/2}}{2(\gamma+1)} (M^2-1)^{1/2} \left(1+\frac{\gamma-1}{2} M^2\right)^{\frac{1}{\gamma-1}} \tag{2.5}$$

This expression is almost identical to that of Bird[7], the main difference being in assuming a constant collision diameter (hard spheres), which we

believe to be commensurate with the overall crudeness of the model. The breakdown surface as defined by equations 2.5 and 2.1, starts at point $[R_B(M_1),\ \psi(M_1)]$ on the exit characteristic $M = M_1$, which we refer to as the intial point (see Figure 4). However, a breakdown in continuum flow also takes place on the segment of the exit characteristic between the corner and the intial point, since the value of the breakdown parameter there (Equation 2.2) is clearly larger than the value of B used in defining the breakdown surface (Equation 2.5). Hence, the breakdown surface defined by (2.5) should be supplemented by that segment. We refer to the combined surface as the augmented breakdown surface. The segment on the exit characteristic is referred to as the supplementary breakdown surface.

The one-sided directed effusion flux is defined as the number flux of molecules per unit area of an area element normal to the flux direction, per unit solid angle about the flux direction. It is obtained as a function of local Mach number and the angle κ between the flux direction and the local velocity vector, by repeating Noller's velocity integration scheme[4,EQ. (6)], with an added factor of molecular speed in order to obtain flux (rather than density as in Noller's work). The resulting expression for species i is readily obtained by using standard definite integrals:

$$
\begin{aligned}
F_i(M) = h_i\, N_o C_o\, (W_A/W_i)^{1/2} \left(1 + \frac{\gamma-1}{2} M^2\right)^{-\frac{\gamma+1}{2(\gamma-1)}} & \\
\left[(2\gamma\pi^3)^{-1/2} \left(1 + (1/2)\gamma\tilde{M}^2\cos^2\kappa\right) \mathrm{EXP}\left(-\gamma\tilde{M}^2/2\right) + \right. & \\
(2\pi)^{-1}\, \tilde{M} \left(3/2 + (1/2)\gamma\tilde{M}^2\cos^2\kappa\right) \cos\kappa\, \mathrm{EXP}\left(-(1/2)\gamma\tilde{M}^2 \sin^2\kappa\right) & \\
\left. \mathrm{ERFC}\left(-(\gamma/2)^{1/2}\, \tilde{M} \cos\kappa\right)\right] &
\end{aligned}
\qquad (2.6)
$$

$$
\mathrm{ERFC}(v) = 2\,\pi^{-1/2} \int_v^\infty \mathrm{EXP}\,(-x^2)dx \qquad \text{(complementary error function)}
$$

$\tilde{M} = (W_i/W_A)^{1/2} M$

h_i - Mole fraction of species i. (2.6 Continued)

W_i - Molecular weight of species i.

The dependence of $F_i(M)$ on the flux angle κ is so sensitive that for some Mach number around $M \approx 10$, the backflow (in the typical operating range) is virtually negligible. In the following section we describe how the flux $F_i(M)$ is integrated over the augmented breakdown surface, yielding the backscattered flux arriving at the surface of the spacecraft.

3. FLUX INTEGRATION

The effusion flux $F_i(M)$ given by (2.6) above, is defined in such a way that the number of molecules effusing from an area element ΔA_B of the breakdown surface and arriving at an area element ΔA_S on the spacecraft (per second), is given by:

$$F_i(M)\ (\Delta A_B\ \text{COS}\ \alpha_B)\ (\Delta A_S\ \text{COS}\alpha_S)\ L_{BS}^{-2}\ \text{[molecules per second]} \qquad (3.1)$$

where α_B, α_S are the angles between the line-of-sight $\vec{L}_{BS}$ (Figure 3) and the normals to the breakdown surface and the spacecraft surface respectively. L_{BS} is the distance between the elements ΔA_B and ΔA_S. Dividing equation (3.1) by ΔA_S and integrating over the breakdown surface, the flux per unit area of the spacecraft is given by:

$$Q_i = \int F_i(M)\text{COS}\alpha_B\ \text{COS}\alpha_S\ L_{BS}^{-2}\ dA_B \quad \text{[Molecules per second per m}^2\text{]} \qquad (3.2)$$

The integration scheme for Q_i over the breakdown surface is expressed in terms of the set of polar coordinates R, ψ, ϕ (Figure 3). For a point (R, ψ, ϕ) on the breakdown surface, using Cartesian coordinates (X, Y, Z) and the angle ω between X-axis and the line-of-sight $\vec{L}_{BS}$ we obtain the following geometrical relationships:

$$X = R\ \text{COS}\psi \ ; \quad Y = (A_o + R\ \text{SIN}\psi)\ \text{COS}\phi \ ; \quad Z = (A_o + R\ \text{SIN}\psi)\text{SIN}\phi$$

$$\text{COS}\phi_{MAX}(M) = \left(\frac{A_o}{A_o + R(M)\text{SIN}\psi}\right) \qquad (3.3)$$

$$\vec{U} = U(\text{COS}\theta,\ \text{SIN}\theta\ \text{COS}\phi,\ \text{SIN}\theta\ \text{SIN}\phi)$$

$$\vec{L}_{BS}/|\vec{L}_{BS}| = (\text{COS}\omega,\ \text{SIN}\omega\ \text{COS}\beta,\ \text{SIN}\omega\ \text{SIN}\beta)$$

$$\text{TAN}\beta = \frac{Z}{(Y - A_o)}$$

The cosines $\cos\kappa$, $\cos\alpha_B$, $\cos\alpha_S$ in (3.2) are expressed as scalar products of $[\vec{L}_{BS}/|\vec{L}_{BS}|]$ and unit vectors along the local velocity vector $\vec{U}$, along the local normal to the breakdown surface and along the local normal to the spacecraft surface, correspondingly.

The integration is performed numerically in two phases, the first being the integration along the supplimentary breakdown surface (Figure 4). For this first phase, the straight line segment which constitutes the supplementary breakdown surface is divided into several intervals of length ΔR (typically 10 intervals). Each interval generates a half-strip by rotating it from $\phi = 0$ through $\phi = \phi_{max}(M_1)$. This strip is in turn subdivided into several sub-intervals of $\Delta\phi$ each (typically 10 intervals). The total flux arriving at X_S is obtained by summing contributions from each sub-interval (two-dimensional integration). When the integration along the supplementary breakdown surface is concluded, it is continued into the breakdown surface, where ΔR intervals are replaced by breakdown surface intervals that correspond to a fixed Mach number increment ΔM (typically $\Delta M=0.1$). The integration proceeds along the breakdown surface (2.5) until the contribution of the last ΔM strip is negligibly small. The computation time is modest (about 1 second CPU per X_S point, on IBM 3033 mainframe computer). The computations were carried out by a code RINGBD written specifically for this purpose. Further details of the scheme and programming can be obtained by reading this code which is given in Appendix A.

4. RESULTS AND DISCUSSION

4.1 Presentation of Results

The molecular flux backscattered to the spacecraft from the surface of continuum flow breakdown in the lip-centered rarefaction fan, has been computed for all five species H, HF, H_2, DF, He. The results are depicted in Figures 5 to 9 respectively. For each species two more cases were computed in addition to the nominal case (1.1), where the stagnation density ρ_o was replaced by $\rho_o/10$ and by ρ_o*10 (see Figures 5 to 9). This has been done in order to demonstrate the effect of variations in exit flow conditions on the flux. The particular choice of ρ_o was motivated by the fact that the effects of changing ρ_o are not obvious. The effects of changing the exit Mach number M_1 or the stagnation temperature T_o are rather obvious (a higher flux would result from either a decrease in M_1 or an increase in T_o). It turns out that for points lying not too near the nozzle lip ($X_s > 0.1$ m), the lower density flow generates a higher backscattered flux!

In addition to varying ρ_o, we also varied the breakdown parameter B, obtaining a surprising result. The computation was performed for a particular species (HF), and the results obtained upon replacing B=0.05 (nominal value) by B/2 and by B*2 are brought in Figure 10.

It turns out that the B/2 case has the higher flux. This is somewhat surprising, since a lower value of B in a centered rarefaction fan (equation 2.5) means that the breakdown of continuum flow takes place in a region further out from the corner. In a source flow (e.g., a spherical source), that implies lower density and temperature, which would give rise to lower thermally backscattered flux.

An explanation to these seemingly counterintuitive results, along with some deeper insight into the breakdown surface model as it is applied to a centered rarefaction flow, can be obtained by taking a close look at the flow field and the breakdown surface in the vicinity of the corner. We take up this matter in the following sections.

We conclude the presentation of results, by comparing the flux (in the nominal case) of the five species with each other (Figure 11). This figure underlines the fact that the flux of light species (H, H_2, He) is many orders of magnitude (typically 10^{15}) times that of heavy species (HF, DF). Indeed, these results demonstrate a well known effect: When an expanding gaseous mixture of light and heavy molecules experiences a breakdown of continuum flow, a separation of species takes place (see e.g., the work of Cattolica et. al. [8]).

4.2 The Breakdown Surface and Streamlines

Consider the parametric description $R_B(M)$ for the breakdown surface (Equation 2.5). Normalizing R relative to the exit mean free path λ_1, we get:

$$R_B(M) = R_B(M_1)\left[(M^2 - 1)/(M_1^2 - 1)\right]^{1/2} \left[\left(1 + \frac{\gamma-1}{2} M^2\right)/\left(1 + \frac{\gamma-1}{2} M_1^2\right)\right]^{\frac{1}{\gamma-1}}$$

$$R_B(M_1)/\lambda_1 = \left[(\gamma\pi/2)^{1/2}/(\gamma+1)B\right] \left(M_1^2 - 1\right)^{1/2} \tag{4.1}$$

$$\lambda_1 = \left(2^{1/2}\pi D^2 N_o\right)^{-1} \left[1 + \frac{\gamma-1}{2} M_1^2\right]^{\frac{1}{\gamma-1}}$$

The normalized surface $R_B(M)/\lambda_1$ is thus independent of stagnation density, depending only on γ, M_1, B.

Let us now derive a parametric equation $R_s(M)$ for a streamline that enters the fan at point $R_s(M_1)$ on the exit characteristic. The following geometrical relationship is readily obtained by considering two characteristic lines ψ and $\psi+\Delta\psi$ and a streamline inclined at the Mach angle μ to them:

$$\frac{dR_s(\psi)}{d\psi} = - R_s(\psi)\ (\tan\mu)^{-1} \tag{4.2}$$

Using the standard Prandtl-Meyer functions (2.1), we get the following differential equation for $R_s(M)$:

$$\frac{1}{R_s(M)}\ \frac{dR_s(M)}{dM} = \left(\frac{\gamma+1}{2}\right) M\left(1 + \frac{\gamma-1}{2} M^2\right)^{-1} \tag{4.3}$$

This equation is readily integrated, giving:

$$R_s(M) = R_s(M_1)\ \left[\left(1 + \frac{\gamma-1}{2} M^2\right)/\left(1 + \frac{\gamma-1}{2} M_1^2\right)\right]^{\frac{\gamma+1}{2(\gamma-1)}} \tag{4.4}$$

As pointed out by Bird[7], there is a particular streamline $R_{sa}(M)$ which asymptotically approaches the breakdown surface for large M, since the ratio $R_s(M)/R_B(M)$ tends to a constant (not zero) when $M \to \infty$. (Strictly speaking, this holds only for hard-sphere molecules, i.e., only when $\omega = 0.5$ in[7]). The limit is:

$$\lim_{M\to\infty} \frac{R_s(M)}{R_B(M)} = \frac{R_s(M_1)}{R_B(M_1)} \left[\frac{M_1^2 - 1}{M_1^2 + \frac{2}{\gamma-1}}\right]^{1/2} \tag{4.5}$$

For the limiting streamline $R_{sa}(M)$, the ratio $R_{sa}(M)/R_B(M)$ should tend to 1. This determines the point $R_{sa}(M_1)$ at which the limiting streamline enters the fan, as well as the entire line $R_{sa}(M)$:

$$R_{sa}(M_1) = R_B(M_1)\ \left[\frac{M_1^2 + \frac{2}{\gamma-1}}{M_1^2 - 1}\right]^{1/2} \tag{4.6}$$

Clearly, $R_{sa}(M)$ is larger than $R_B(M)$ for any $M > M_1$, so that no streamline beyond $R_{sa}(M)$ can cross the breakdown surface. This pattern is shown in Figure 4, where $R_{sa}(M)$ is denoted "streamline 2", and "streamline 1" is the streamline $R_S(M_1) = R_B(M_1)$.

All this leads to the following observation regarding the continuum breakdown of the flow in a centered rarefaction fan[7]. Referring to Figure 4, the fluid entering the fan through the supplementary breakdown surface (i.e., through the exit characteristic between the corner and the initial point of streamline 1), experiences breakdown immediately upon crossing this surface. Every streamline between streamline 1 and streamline 2 crosses the breakdown surface at some Mach number $M > M_1$, and at that point the continuum flow breaks down. All fluid entering the fan beyond streamline 2 will never pass through the breakdown surface, and hence will maintain a continuum flow regime all the way to infinity. Of course, that is only true for planar centered rarefaction fans. When the exhaust flow emerges from a nozzle of finite width, and especially when the exhaust jet has a ring symmetry (as in our case), the breakdown surface gradually curves in a balloonlike shape towards the opposite nozzle lip, forming the familiar plume pattern (Figure 1).

4.3 Analysis and Discussion of Results

The foregoing analysis is now used to explain the variation in back-scattered flux due to a change in exhaust flow conditions at the nozzle exit. Specifically, we consider a tenfold decrease in stagnation density (i.e., the case $\rho_o/10$), and hence a tenfold increase in the exit mean free path λ_1.

The effusion flux from the breakdown surface is proportional to the local density, so one would expect to observe a decrease in flux, rather than

an increase (see Figures 5 to 9, for $X_s > 0.1$ m). Other factors causing increased flux, must then be larger than 10 so that they more than offset the 1/10 factor in density. It turns out that these effects are mainly geometrical, in that a tenfold increase in λ_1 causes the domain of integration on the breakdown surface to increase more than tenfold. In the (X,Y) plane there is a tenfold "blowup" of the breakdown surface, due to the self-similar structure of the Prandtl-Meyer flow field. As a result of this "blowup" in (X,Y), the angular integration range ϕ_{max} also increases, albeit not linearly (Equation 3.3). Another geometrical effect is an increase in the flux incidence cosine factor $\cos\alpha_s$ (see Equation 3.2), which for points X_s sufficiently far from the nozzle lip, increases roughly tenfold (while the other cosine factor $\cos^{\alpha}{}_B$ is almost constant). All this provides a qualitative explanation for the observed increase in flux at far points ($X_s >$ 0.1 m).

As for the near range ($X_s < 0.1$ m), another effect becomes increasingly significant as X_s approaches the nozzle lip. The turning angle κ, by which backscattered molecules have to be deflected relative to the flow velocity vector in order to reach point X_s on the spacecraft (Figure 2), increases with the size of the breakdown surface (fixed M and X_s). Since the local effusion flux (Equation 2.6) decreases rather sharply as κ is increased, the net result is a tendency to get a reduced backscattered flux at near points such as X_s = 0.01 m (Figures 5 to 9).

We now turn to the effect of changing the value of the breakdown parameter B. From equation 4.1 it is clear that multiplying B by some factor

will have the same "blowup" effect as dividing λ_1 by the same factor. A tenfold decrease in B is thus geometrically equivalent to a tenfold decrease in ρ_o. However, since the local effusion flux at the breakdown surface is proportional to ρ_o while it is independent of B, the B/10 case will have ten times as much backscattered flux as the $\rho_o/10$ case. In order to illustrate the sensitivity of the flux estimates to an uncertainty in the appropriate value of B, we computed the cases B/2 and B*2 for one species (HF), and they are presented in Figure 10. The variation in flux relative to the nominal case (B = 0.05), is by a factor no larger than about 5. Results for other species were found to exhibit comparable variations.

Does this observation about the dependence of the breakdown surface on B agree with the breakdown surface appropriate to the far field of the exhaust plume? In stationary source flow into vacuum, and when $M \gg 1$, the breakdown parameter varies with radius as $B \sim R^{\delta-1}$ ($\delta = 1$ for cylindrical source, $\delta = 2$ for spherical source). In a ringjet, the stream tubes of the exhaust plume generally diverge at a rate higher than that of stream tubes in a cylindrical source flow, so the effective value of δ in a ringjet is $\delta > 1$. Hence, in this case the far field breakdown surface moves downstream along each stream tube as the value of B increases. This is indeed geometrically compatible with the fact that near the corner of the lip-centered rarefaction fan $B \sim R^{-1}$, as shown schematically in Figure 12. The dependence of the breakdown surface on B near the corner and in the far field, thus assures that complete breakdown surfaces corresponding to different values of B, do not intersect (Figure 12).

In the foregoing discussion it was pointed out that variations in flux caused by changes in parameters such as ρ_o and B, were directly related

to the self-similar structure of the Prandtl-Meyer flow field. It has been further shown that these variations are well-understood within the framework of the breakdown surface model and that they are not excessively large. Are we to conclude that the thermally backscattered flux estimates of the present model are also physically plausible and reliable? In the following section we take up this matter, arriving at some interesting conclusions about this model and its range of validity.

4.4 Critical Examination of the Model

Consider the centered rarefaction flow field of a compressible fluid negotiating an expansive corner at supersonic speed (Prandtl-Meyer flow). The streamlines of this flow field have an orderly "layered" structure, with each streamline curving around the corner, starting at its point of entrance into the fan (see Figure 4).

The present model is based on the stipulation that there is a point of continuum flow breakdown on each streamline, provided this streamline is not beyond a certain limiting streamline. Consider a sample molecule effusing from this breakdown point toward the spacecraft. It advances at constant speed along a straight line trajectory, traversing all inner streamlines. Since the flow velocity vector points away from the spacecraft, and since the flow is highly supersonic so that the velocity of most individual molecules does not differ much from the flow velocity (i.e., it is a "cold" flow), any collision of the sample molecule with a mainflow molecule will most probably divert the sample molecule away from the spacecraft. What is the probability that a sample molecule would traverse this cross flow collisionlessly? This probability is simply $\exp(-n)$, where n is the expected number of collisions along the straight-line trajectory from the point of breakdown to the spacecraft. In the typical operating conditions assumed here, we estimated n to be roughly about 10. Since this no-collision probability factor is ignored in the formulation of the present model, the backscattered flux may be exaggerated by a factor of $\exp(10)$ or about 10^4. We conclude that in all likelihood, the prediction of the breakdown surface model for thermally backscattered flux from a centered rarefaction flow, is substantially overestimated.

Can anything be done to improve the present model? One may be inclined to suggest at this point that the obvious remedy is to incorporate the no-collision probability factor into the model. Rather, we prefer to retain the breakdown surface model in its present form as a simple means of obtaining an overestimate to the thermally backscattered flux from a centered rarefaction flow. An improved model can be constructed by considering thermal backscattering from the entire flow field (tempered by the probability of no-collision), without resorting to the physically untenable notion of an abrupt transition from continuum flow to free molecular flow.

5. CONCLUSIONS

Some surprising similarity laws of the breakdown surface model were observed. It has been shown that they were a direct result of the self similar structure of the Prandtl-Meyer flow field to which the model was applied. Specifically, it was found (and shown plausible) that reduced values of either the exhaust stagnation density ρ_o, or the breakdown parameter B, caused higher backscattered flux.

The breakdown surface model for thermally backscattered flux from a centered rarefaction fan, has been shown to overestimate the flux arriving at the spacecraft. It is suggested that an improved model be constructed by considering thermal backscattering from the entire flow field, along with the probability factor for a side-scattered molecule traversing the main flow collisionlessly.

The molecular flux of corrosive species (HF, DF) arriving at the spacecraft (Figures 6 and 8) is no larger than about 10^7 (sec^{-1} m^{-2}), which is negligible since it corresponds to about 10^{-5} molecular monolayers per year. This conclusion is reliable since even this flux level is an overestimate.

The maximum thermally backscattered flux of light species (H, H_2, He) is in the range of 10^{20} to 10^{22} (sec^{-1} m^{-2}) (see Figures 5, 7, 9). Thus, we conclude that while thermal backscattering would contribute significantly to the flux of light molecules arriving at the spacecraft, it is utterly negligible as far as heavy molecules are concerned.

5. REFERENCES

(1) Chemical Propulsion Information Agency, "JANNAF Handbook, Rocket Exhaust Plume Technology, Chapter 6: Spacecraft Plume Contamination", CPIA Publication 263, June 1983.

(2) Chemical Propulsion Information Agency, "JANNAF 13th Plume Technology Meeting," Vol. I, Houston, TX, April 1982. CPIA Publication 357, April 1982.

(3) G. A. Bird, "Breakdown of Continuum Flow in Free Jets and Rocket Plumes", Proc. 12th Symp. on Rarefied Gas Dynamics. In Vol. 74, Progress in Aeronautics and Astronautics, Sam S. Fisher Editor, Published by AIAA 1981.

(4) H. B. Noller, "Approximate Calculation of Expansion of Gas From Nozzles into High Vacuum", The Journal of Vacuum Science and Technology, Vol. 3, 202-207, 1966.

(5) F. Mastrup, E. Broadwell, J. Miller and T. A. Jacobs, "Hydrogen Fluoride Laser Technology Study", Technical Report No. AFWL-TR-72-28, October 1972.

(6) G. A. Bird, Molecular Gas Dynamics, Clarendon Press, Oxford 1976.

(7) G. A. Bird, "Prandtl-Meyer Flow of a Finite Knudsen Number Gas", Proceedings of the Seventh Australian Conference on Hydrodynamics and Fluid Mechanics, 1980.

(8) R. J. Cattolica, R. J. Gallagher, J. B. Anderson and L. Talbot, "Aerodynamic Separation of Gases by Velocity Slip in Freejet Expansions", AIAA Journal, Vol. 17, P. 344, 1974. (Also Reprint AIAA-77-709).

APPENDIX A. The Computer Code RINGBD

We present a printout of the code RINGBD along with the reults of the nominal case (printout of actual run). This is preceded by a brief description of the subroutines and a summary of major variables with their code and report notations.

A.1 Description of Subroutines

MAIN PROGRAM - Computes flux integration by summation of segment contributions (centered). Printing of results.

INIDAT - Definition of all data (no input file). Preparatory evaluation of parameters. Printing of data.

FLUX - Evaluates flux emitted from a single point on breakdown surface (mean segment values) to a point on spacecraft (XS).

BREAKR - Computes point on breakdown surface for given Mach number.

BREAKM - Computes point on breakdown surface for mean Mach number of a segment.

A.2 Code Versus Report Notation

XC(I) - [AB] - Mole fraction of species AB. (I=1,2,3,4,5 corresponds to H, HF, H_2, DF, He).

WC(I) - W_i - Molecular weight of species i.

WAV - W_A - Average molecular weight

TO - T_o - Stagnation temperature

RHOO - ρ_o - Stagnation density

G - γ - Specific heat ratio

EM1 - M_1 - Exit Mach number

LAMDA1 - λ_1 - Exit mean free path

AO - A_o - Spacecraft radius

R - R - Distance from corner ($X=0$, $Y^2+Z^2 = A_o^2$).

DIST - L_{BS} - Distance between emitting point on breakdown surface and receiving point (XS) on spacecraft.

XS - X_s - Point on spacecraft ($X=X_s$, $Y=A_o$, $Z=0$).

PSI - ψ - Characteristic angle

AMU - μ - Mach angle

TETA - θ - Velocity vector angle

PHI - ϕ - Rotation angle for flux integration

W - ω - Angle between x-axis and line-of-sight $\vec{L}_{BS}$

BETA - β - Angle between Y-axis and projection of $\vec{L}_{Bs}$ on (Y,Z) plane.

DMO - ΔM - Mach number increment for flux integration

EM - M - Mach number

PBIRD - B - Breakdown parameter

A.3 Code Listing (Run of Nominal Case):

```
      $JOB            RINGBD,NOXREF                                                  RIN00010
 1          IMPLICIT REAL*8(A-H,O-Z,$)                                              RIN00020
 2          COMMON /GAMA/G,G1,G2,G3,G4,G5,G6,G7,G8,G9,G10,G11,G12,G13,G14,G15,RIN00030
           1            G16,G17,G18,G19,G20                                        RIN00040
 3          COMMON /PAR/C0,EN0,EM1,D,TLIM,ETALIM,CLIM,EL0,Q0,T0,                    RIN00050
           1           PBIRD,RBIRD,DM0,DEG,OMEGA,XSV(51)                          RIN00060
 4          COMMON /NPAR/NETA,NC,NT,NEM0,NPHI,NXS,NR0,NSPEC                         RIN00070
 5          COMMON /GEOM/APF,PAI,PAI2,SW,CW,BETA,SBETA,CBETA,PSI1,SPSI1,            RIN00080
           1            CPSI1,PSIF,SPSIF,CPSIF,AK,SK,CK,A0,RF,XF,YF,ZF,            RIN00090
           2            PHI,SPHI,CPHI,RMIN,RMAX,XS,DIST,                           RIN00100
           3            AMU1,ZETA1,XN,YN,ZN,PSIM,SPSIM,CPSIM,R0                    RIN00110
 6          COMMON /EPSIL/EPSQ,EPSETA,EPST,EPSC,EPSEM                               RIN00120
 7          COMMON /EXTREM/TEXT,ETAEXT,CEXT,REXT,PSIEXT,EMEXT,BEXT,QEXT            RIN00130
 8          COMMON /SPEC/WAV,XC(5),WC(5),WCR(5),XNAME(5),QC(5),FLUXC(5)             RIN00140
 9          DIMENSION DSUM(5)                                                       RIN00150
10          PRINT 101                                                               RIN00160
11     101  FORMAT('1'/1X,'RINGBD - FLUX INTEGRATION FROM BREAKDOWN',               RIN00170
           1           1X,'SURFACE'//)                                            RIN00180
      C                                                                            RIN00190
12          CALL INIDAT                                                             RIN00200
      C                                                                            RIN00210
13          PRINT 110,XNAME                                                         RIN00220
14     110  FORMAT(///1X,'  NX',' NEM','    XS   ',' PHIMAX','    QMAX   ',      RIN00230
           1           5(4X,A6,1X,'/ LOG',1X))                                    RIN00240
15          DO 200 NX=1,NXS                                                         RIN00250
16          EM=EM1                                                                  RIN00260
17          CALL BREAKR(EM,RF)                                                      RIN00270
18          IF(NR0.GT.0) RF=R0                                                      RIN00280
19          XF=RF*CPSI1                                                             RIN00290
20          YF=RF*SPSI1+A0                                                          RIN00300
21          XS=XSV(NX)                                                              RIN00310
22          QMAX=0.                                                                 RIN00320
23          DO 45 N=1,NSPEC                                                         RIN00330
24          FLUXC(N)=0.                                                             RIN00340
25     45   CONTINUE                                                                RIN00350
26          DO 1 NEM=1,NEM0                                                         RIN00360
27          RN=RF                                                                   RIN00370
28          XN=XF                                                                   RIN00380
29          YN=YF                                                                   RIN00390
30          IF(NEM.GT.NR0) GO TO 41                                                 RIN00400
31          RF=R0+DFLOAT(NEM)*(RMIN-R0)/DFLOAT(NR0)                                 RIN00410
32          XF=RF*CPSI1                                                             RIN00420
33          YF=RF*SPSI1+A0                                                          RIN00430
34          RMEAN=(RN+RF)/2.D0                                                      RIN00440
35          EMMEAN=EM1                                                              RIN00450
36          PSIM=PSI1                                                               RIN00460
37          SPSIM=SPSI1                                                             RIN00470
38          CPSIM=CPSI1                                                             RIN00480
39          GO TO 42                                                                RIN00490
40     41   CONTINUE                                                                RIN00500
41          EM=EM+DM0                                                               RIN00510
42          CALL BREAKR(EM,RF)                                                      RIN00520
43          EMMEAN=EM-DM0/2.D0                                                      RIN00530
44          CALL BREAKM(EMMEAN,RMEAN)                                               RIN00540
45     42   CONTINUE                                                                RIN00550
46          ALONG=DSQRT((XF-XN)**2+(YF-YN)**2)                                      RIN00560
47          SALFA=(YF-YN)/ALONG                                                     RIN00570
48          CALFA=(XF-XN)/ALONG                                                     RIN00580
49          PHIMAX=DARCOS(A0/(A0+RMEAN*SPSIM))                                      RIN00590
50          DPHI=PHIMAX/NPHI                                                        RIN00600
```

```
51          DO 44 N=1,NSPEC                                                    RIN0061
52          DSUM(N)=0.                                                         RIN0062
53     44   CONTINUE                                                           RIN0063
54          DO 2 NP=1,NPHI                                                     RIN0064
55          PHI=(DFLOAT(NP)-0.5D0)*DPHI                                        RIN0065
56          CALL FLUX(EMMEAN,RMEAN)                                            RIN0066
57          CROSS1=SW*CBETA                                                    RIN0067
58          CROSS2=(SALFA)*(-CW)+(-CALFA*CPHI)*(-SW*CBETA)+                    RIN0068
           1       (-CALFA*SPHI)*(-SW*SBETA)                                   RIN0069
59          GOREM=CROSS1*CROSS2*DPHI*(A0+RMEAN*SPSIM)*ALONG/DIST**2            RIN0070
60          DO 24 N=1,NSPEC                                                    RIN0071
61          DSUM(N)=DSUM(N)+QC(N)*GOREM                                        RIN0072
62     24   CONTINUE                                                           RIN0073
63          IF(QMAX.GE.QEXT) GO TO 25                                          RIN0074
64          QMAX=QEXT                                                          RIN0075
65     25   CONTINUE                                                           RIN0076
C           PRINT 22,NEM,NP,EMMEAN,RMEAN,PHIMAX*DEG,DARCOS(CW)*DEG,            RIN0077
C          1          BETA*DEG,PHI*DEG,CROSS1,CROSS2,ALONG,DIST,GOREM,        RIN0078
C          2          SPSIM,A0,(QC(N),FLUXC(N),N=1,NSPEC)                     RIN0079
C22        FORMAT(/1X,'NEM,NP,EMMEAN,RMEAN,PHIMAX=',2I3,3D13.4/               RIN0080
C          1       1X,'W,BETA,PHI=',3D15.5/                                   RIN0081
C          2       1X,'CROSS1,CROSS2,ALONG,DIST,GOREM=',5D15.5/               RIN0082
C          3       1X,'SPSIM,A0=',2D15.5/                                     RIN0083
C          4       1X,'QC,FLUXC=',5(1X,D10.3,1X,D10.3))                       RIN0084
66     2    CONTINUE                                                           RIN0085
67          DO 26 N=1,NSPEC                                                    RIN0086
68          FLUXC(N)=FLUXC(N)+DSUM(N)                                          RIN0087
69     26   CONTINUE                                                           RIN0088
70          IF(NEM.LE.NR0+2) GO TO 1                                           RIN0089
71          DO 27 N=1,NSPEC                                                    RIN0090
72          IF((DSUM(N)/FLUXC(N)).GT.EPSEM) GO TO 28                           RIN0091
73     27   CONTINUE                                                           RIN0092
74          GO TO 10                                                           RIN0093
75     28   CONTINUE                                                           RIN0094
76     1    CONTINUE                                                           RIN0095
77     10   CONTINUE                                                           RIN0096
78          DO 31 N=1,NSPEC                                                    RIN0097
79          FLUXC(N)=2.D0*XC(N)*FLUXC(N)                                       RIN0098
80     31   CONTINUE                                                           RIN0099
81          PRINT 11,NX,NEM,XS,PHIMAX*DEG,QMAX,                                RIN0100
           1       (FLUXC(N),DABS(DLOG10(FLUXC(N))),N=1,NSPEC)                 RIN0101
82     11   FORMAT(/1X,2I4,F9.4,F7.2,D11.3,5(1X,D10.3,'/',F5.2))               RIN0102
83     200  CONTINUE                                                           RIN0103
84          PRINT 102                                                          RIN0104
85     102  FORMAT(///1X,'END RINGBD RUN',///)                                 RIN0105
86          STOP                                                               RIN0106
87          END                                                                RIN0107

88          SUBROUTINE INIDAT                                                  RIN0108
89          IMPLICIT REAL*8(A-H,O-Z,$)                                         RIN0109
90          REAL*8 LAMDA0,LAMDA1                                               RIN0110
91          COMMON /GAMA/G,G1,G2,G3,G4,G5,G6,G7,G8,G9,G10,G11,G12,G13,G14,G15,  RIN0111
           1            G16,G17,G18,G19,G20                                    RIN0112
92          COMMON /PAR/C0,EN0,EM1,D,TLIM,ETALIM,CLIM,EL0,Q0,T0,               RIN0113
           1           PBIRD,RBIRD,DM0,DEG,OMEGA,XSV(51)                       RIN0114
93          COMMON /NPAR/NETA,NC,NT,NEM0,NPHI,NXS,NR0,NSPEC                    RIN0115
94          COMMON /GEOM/APF,PAI,PAI2,SW,CW,BETA,SBETA,CBETA,PSI1,SPSI1,       RIN0116
           1            CPSI1,PSIF,SPSIF,CPSIF,AK,SK,CK,A0,RF,XF,YF,ZF,       RIN0117
           2            PHI,SPHI,CPHI,RMIN,RMAX,XS,DIST,                      RIN0118
           3            AMU1,ZETA1,XN,YN,ZN,PSIM,SPSIM,CPSIM,R0               RIN0119
```

```
 95          COMMON /EPSIL/EPSQ,EPSETA,EPST,EPSC,EPSEM                          RIN01200
 96          COMMON /EXTREM/TEXT,ETAEXT,CEXT,REXT,PSIEXT,EMEXT,BEXT,QEXT        RIN01210
 97          COMMON /SPEC/WAV,XC(5),WC(5),WCR(5),XNAME(5),QC(5),FLUXC(5)         RIN01220
 98          DATA XC/.091D0,.091D0,.104D0,.135D0,.579D0/                         RIN01230
 99          DATA WC/1.00D0,20.0D0,2.00D0,21.0D0,4.00D0/                         RIN01240
100          DATA XNAME/'   H  ','  HF  ','  H2  ','  DF  ','  HE  '/           RIN01250
101          PAI=4.*DATAN(.1D 1)                                                 RIN01260
102          AR=8.3143D3                                                         RIN01270
103          AV=6.022D 26                                                        RIN01280
       C  OMEGA=0.5 IS FOR HARD SPHERE COLLISIONS,                               RIN01290
       C  AN AVERAGE RECOMMENDED VALUE IS ABOUT OMEGA=0.75                       RIN01300
104          OMEGA=0.5D0                                                         RIN01310
105          NSPEC=5                                                             RIN01320
106          WAV=0.                                                              RIN01330
107          DO 51 N=1,NSPEC                                                     RIN01340
108          WAV=WAV+XC(N)*WC(N)                                                 RIN01350
109      51  CONTINUE                                                           RIN01360
110          DO 52 N=1,NSPEC                                                     RIN01370
111          WCR(N)=DSQRT(WC(N)/WAV)                                             RIN01380
112      52  CONTINUE                                                           RIN01390
113          A0=2.5D0                                                            RIN01400
114          EM1=4.0D0                                                           RIN01410
115          RHO0=0.0075D0                                                       RIN01420
116          T0=2.300D3                                                          RIN01430
117          D=2.50D-10                                                          RIN01440
118          G=1.54D0                                                            RIN01450
119          EN0=RHO0*AV/WAV                                                     RIN01460
120          C0=DSQRT(G*AR*T0/WAV)                                               RIN01470
121          PBIRD=0.05D0*2.D0                                                   RIN01480
       C  R0 IS THE RADIUS FOR BEGINNING THE INTEGRATION ALONG THE M=M1          RIN01490
       C  CHARACTERISTIC(THE AUGMENTED BREAKDOWN SURFACE).                       RIN01500
       C  NR0 IS THE NUMBER OF INTEGRATION INTERVALS ON THIS SEGMENT.            RIN01510
       C  FOR NO INTEGRATION ALONG M=M1 CHARACTERISTIC, SET NR0=0.               RIN01520
122          R0=0.                                                               RIN01530
123          NR0=10                                                              RIN01540
124          DM0=0.1D0                                                           RIN01550
125          NEM0=20.D0/DM0+NR0                                                  RIN01560
       C  TO GET FLUX DUE TO AUGMENTED BREAKDOWN SURFACE SOLELY, ACTIVATE:       RIN01570
       C     NEM0=NR0                                                           RIN01580
126          NPHI=10                                                             RIN01590
127          NXS=13                                                              RIN01600
128          XSI=1.D-2                                                           RIN01610
129          XSF=1.D1                                                            RIN01620
130          XSV(1)=XSI                                                          RIN01630
131          IF(NXS.EQ.1) GO TO 111                                              RIN01640
132          DXL=(DLOG(XSF)-DLOG(XSI))/(NXS-1.D0)                                RIN01650
133          XLI=DLOG(XSI)                                                       RIN01660
134          DO 11 NX=2,NXS                                                      RIN01670
135          XSV(NX)=DEXP(XLI+(NX-1.D0)*DXL)                                     RIN01680
136      11  CONTINUE                                                           RIN01690
137      111 CONTINUE                                                           RIN01700
138          EPSEM=1.D-5                                                         RIN01710
139          DEG=180.D0/PAI                                                      RIN01720
140          PAI2=PAI/2.D0                                                       RIN01730
141          GAMMA=G                                                             RIN01740
142          G1=(G-1.D0)/2.D0                                                    RIN01750
143          G2=(G+1.D0)/(2.D0*(G-1.D0))                                         RIN01760
144          G3=G/2.D0                                                           RIN01770
145          G4=(G+1.D0)/(G-1.D0)                                                RIN01780
146          G5=DSQRT((G+1.D0)/(G-1.D0))                                         RIN01790
```

```
      G6=1.D0/(G-1.D0)                                                  RIN018
      G7=2.D0/(G+1.D0)                                                  RIN018
      G8=(5.D-1*(G+1.D0)**2/(G-1.D0))**(1.D0/(G+1.D0)) *                RIN018
     1   ((G+1.D0)/(G-1.D0))**((G-1.D0)/(G+1.D0))                       RIN018
      G9=(G+3.D0)/(2.D0*(G-1.D0))                                       RIN018
      G10=(7.D0-3.D0*G)/(2.D0*(G-1.D0))                                 RIN018
      G11=DSQRT(G/PAI)/(2.D0*(G+1.D0))                                  RIN018
      G12=DSQRT(G/2.D0)                                                 RIN018
      G13=1.D0/DSQRT(2.D0*G*PAI**3)                                     RIN018
      LAMDA0=1.D0/(DSQRT(2.D0)*PAI*D**2*EN0)                            RIN018
      LAMDA1=LAMDA0*(1.D0+G1*EM1**2)**(G6-OMEGA+0.5D0)                  RIN019
      RBIRD=G11/(D**2*EN0*PBIRD)                                        RIN019
      ZETA1=G5*DATAN(DSQRT(EM1**2-1.D0)/G5)                             RIN019
      AMU1=DARSIN(1.D0/EM1)                                             RIN019
      PSI1=PAI2+AMU1                                                    RIN019
      SPSI1=DSIN(PSI1)                                                  RIN019
      CPSI1=DCOS(PSI1)                                                  RIN019
      PSIF=PAI2+AMU1+ZETA1-G5*PAI2                                      RIN019
      SPSIF=DSIN(PSIF)                                                  RIN019
      CPSIF=DCOS(PSIF)                                                  RIN019
      CALL BREAKR(EM1,RMIN)                                             RIN020
      RSMIN=RMIN*DSQRT((2.D0/(G-1.D0)+EM1**2)/(EM1**2-1.D0))            RIN020
C                                                                       RIN020
      PRINT 201,NSPEC,XNAME                                             RIN020
  201 FORMAT(/1X,'SPECIES DATA   NSPEC=',I3/                            RIN020
     1        1X,'SPECIES NAMES    ',11(2X,A6,2X))                     RIN020
      PRINT 202,XC                                                      RIN020
  202 FORMAT( 1X,'MOLE FRACTION XC=',11(F8.4,2X))                       RIN020
      PRINT 203,WC                                                      RIN020
  203 FORMAT( 1X,'MOL. WEIGHT   WC=',11(F8.4,2X))                       RIN020
      PRINT 21,AR,AV,WAV,G,RHO0,T0,EN0,C0,D                             RIN021
   21 FORMAT(/1X,'THERMODYNAMIC DATA'/                                  RIN021
     1        1X,'AR,AV,WAV,GAMMA=',2X,2D14.5,2F9.3/                    RIN021
     2        1X,'RHO0,T0,EN0,C0,D=',D12.4,F8.0,D13.5,2D12.4)           RIN021
      PRINT 22,EM1,PSI1*DEG,PSIF*DEG,PBIRD,                             RIN021
     1         A0,RMIN,RSMIN,R0,                                        RIN021
     2         LAMDA0,LAMDA1,RMIN/LAMDA1,RSMIN/LAMDA1                   RIN021
   22 FORMAT(/1X,'FLOW AND GEOMETRY DATA'/                              RIN021
     1        1X,'EM1,PSI1,PSIF,PBIRD=',4F9.3/                          RIN021
     2        1X,'A0,RMIN,RSMIN,R0=',F9.3,3D14.5/                       RIN021
     3        1X,'LAMDA0,LAMDA1,RMIN/LAMDA1,RSMIN/LAMDA1=',4D13.4)      RIN022
      PRINT 23,DM0,NPHI,NR0,EPSEM                                       RIN022
   23 FORMAT(/1X,'INTEGRATION DATA'/                                    RIN022
     1        1X,'DM0,NPHI,NR0,EPSEM=',F9.3,2I5,4X,D12.3)               RIN022
      RETURN                                                            RIN022
      END                                                               RIN022

      SUBROUTINE FLUX(EM,R)                                             RIN022
      IMPLICIT REAL*8(A-H,O-Z,$)                                        RIN022
      COMMON /GAMA/G,G1,G2,G3,G4,G5,G6,G7,G8,G9,G10,G11,G12,G13,G14,G15,RIN022
     1            G16,G17,G18,G19,G20                                   RIN022
      COMMON /PAR/C0,EN0,EM1,D,TLIM,ETALIM,CLIM,EL0,Q0,T0,              RIN023
     1           PBIRD,RBIRD,DM0,DEG,OMEGA,XSV(51)                      RIN023
      COMMON /NPAR/NETA,NC,NT,NEM0,NPHI,NXS,NR0,NSPEC                   RIN023
      COMMON /GEOM/APF,PAI,PAI2,SW,CW,BETA,SBETA,CBETA,PSI1,SPSI1,      RIN023
     1             CPSI1,PSIF,SPSIF,CPSIF,AK,SK,CK,A0,RF,XF,YF,ZF,      RIN023
     2             PHI,SPHI,CPHI,RMIN,RMAX,XS,DIST,                     RIN023
     3             AMU1,ZETA1,XN,YN,ZN,PSIM,SPSIM,CPSIM,R0              RIN023
      COMMON /EXTREM/TEXT,ETAEXT,CEXT,REXT,PSIEXT,EMEXT,BEXT,QEXT      RIN023
      COMMON /SPEC/WAV,XC(5),WC(5),WCR(5),XNAME(5),QC(5),FLUXC(5)       RIN023
```

```
190          SPHI=DSIN(PHI)                                                    RIN02390
191          CPHI=DCOS(PHI)                                                    RIN02400
192          XMEAN=R*CPSIM                                                     RIN02410
193          YMEAN=(A0+R*SPSIM)*CPHI                                           RIN02420
194          ZMEAN=(A0+R*SPSIM)*SPHI                                           RIN02430
195          TBETA=ZMEAN/(YMEAN-A0)                                            RIN02440
196          BETA=PAI2-DATAN(1.D0/TBETA)                                       RIN02450
197          SBETA=DSIN(BETA)                                                  RIN02460
198          CBETA=DCOS(BETA)                                                  RIN02470
199          DIST=DSQRT((XS-XMEAN)**2+(YMEAN-A0)**2+ZMEAN**2)                  RIN02480
200          CW=-(XS-XMEAN)/DIST                                               RIN02490
201          SW=DSQRT(1.D0-CW**2)                                              RIN02500
202          GM=(1.D0+G1*EM**2)**(-G2)                                         RIN02510
203          AMU=DARSIN(1.D0/EM)                                               RIN02520
204          TETA=PSIM-AMU                                                     RIN02530
205          STETA=DSIN(TETA)                                                  RIN02540
206          CTETA=DCOS(TETA)                                                  RIN02550
207          CKAPA=(CTETA)*(-CW)+(STETA*CPHI)*(-SW*CBETA)+                     RIN02560
            1       (STETA*SPHI)*(-SW*SBETA)                                   RIN02570
208          SKAPA=DSQRT(1.D0-CKAPA**2)                                        RIN02580
209          QEXT=0.                                                           RIN02590
210          DO 1 N=1,NSPEC                                                    RIN02600
211          EMT=EM*CKAPA*G12*WCR(N)                                           RIN02610
212          IF(DABS(EMT).GT.13.D0) EMT=EMT*(13.D0/DABS(EMT))                  RIN02620
213          POW=G3*EM**2*WCR(N)**2                                            RIN02630
214          POWT=POW*SKAPA**2                                                 RIN02640
215          IF(POW.GT.1.0D2)POW=1.0D2                                         RIN02650
216          IF(POWT.GT.1.0D2) POWT=1.0D2                                      RIN02660
217          EXP1=DEXP(-POW)                                                   RIN02670
218          EXP2=DEXP(-POWT)                                                  RIN02680
219          ERFC1=DERFC(-EMT)                                                 RIN02690
220          IF(ERFC1.LT.1.D-43) ERFC1=1.D-43                                  RIN02700
     C       IF(XS.LT.5.D0) GO TO 234                                          RIN02710
     C       IF(EXP1.GT.1.D-20.AND.ERFC1.GT.1.D-20) GO TO  234                 RIN02720
     C       PRINT 235,N,POW,POWT,EMT,EXP1,EXP2,ERFC1                          RIN02730
     C235    FORMAT(I4,8D11.3)                                                 RIN02740
     C234    CONTINUE                                                          RIN02750
221          EVER1=EN0*(C0/WCR(N))*G13*GM*(1.D0+EMT**2)*EXP1                   RIN02760
222          EVER2=(EN0*(C0/WCR(N))*0.5D0/PAI)*(EM*WCR(N))*CKAPA*GM*           RIN02770
            1       (1.5D0+EMT**2)*EXP2*ERFC1                                  RIN02780
223          QC(N)=EVER1+EVER2                                                 RIN02790
224          IF(QEXT.GE.QC(N)) GO TO 1                                         RIN02800
225          QEXT=QC(N)                                                        RIN02810
226      1   CONTINUE                                                          RIN02820
227          RETURN                                                            RIN02830
228          END                                                               RIN02840

229          SUBROUTINE BREAKR(EM,R)                                           RIN02850
230          IMPLICIT REAL*8(A-H,O-Z,$)                                        RIN02860
231          COMMON /GEOM/APF,PAI,PAI2,SW,CW,BETA,SBETA,CBETA,PSI1,SPSI1,      RIN02870
            1             CPSI1,PSIF,SPSIF,CPSIF,AK,SK,CK,A0,RF,XF,YF,ZF,     RIN02880
            2             PHI,SPHI,CPHI,RMIN,RMAX,XS,DIST,                    RIN02890
            3             AMU1,ZETA1,XN,YN,ZN,PSIM,SPSIM,CPSIM,R0             RIN02900
232          COMMON /PAR/C0,EN0,EM1,D,TLIM,ETALIM,CLIM,EL0,Q0,T0,              RIN02910
            1           PBIRD,RBIRD,DM0,DEG,OMEGA,XSV(51)                      RIN02920
233          COMMON /GAMA/G,G1,G2,G3,G4,G5,G6,G7,G8,G9,G10,G11,G12,G13,G14,G15,RIN02930
            1             G16,G17,G18,G19,G20                                  RIN02940
234          R=RBIRD*DSQRT(EM**2-1.D0)*(1.D0+G1*EM**2)**(G6-OMEGA+0.5D0)       RIN02950
235          ZETA=G5*DATAN(DSQRT(EM**2-1.D0)/G5)                               RIN02960
236          PSI=PAI2+AMU1+ZETA1-ZETA                                          RIN02970
```

```
237           XF=R*DCOS(PSI)                                                    RIN02980
238           YF=R*DSIN(PSI)+A0                                                 RIN02990
239           ZF=0.                                                             RIN03000
240    1      CONTINUE                                                          RIN03010
241           RETURN                                                            RIN03020
      C                                                                        RIN03030
242           ENTRY BREAKM(EM,R)                                                RIN03040
      C                                                                        RIN03050
243           R=RBIRD*DSQRT(EM**2-1.D0)*(1.D0+G1*EM**2)**(G6-OMEGA+0.5D0)       RIN03060
244           ZETA=G5*DATAN(DSQRT(EM**2-1.D0)/G5)                               RIN03070
245           PSIM=PAI2+AMU1+ZETA1-ZETA                                         RIN03080
246           SPSIM=DSIN(PSIM)                                                  RIN03090
247           CPSIM=DCOS(PSIM)                                                  RIN03100
248           RETURN                                                            RIN03110
249           END                                                               RIN03120

      $ENTRY                                                                   RIN03130
```

```
RINGBD - FLUX INTEGRATION FROM BREAKDOWN SURFACE


SPECIES DATA   NSPEC=  5
SPECIES NAMES          H          HF          H2          DF          HE
MOLE FRACTION XC=   0.0910     0.0910     0.1040     0.1350     0.5790
MOL. WEIGHT   WC=   1.0000    20.0000     2.0000    21.0000     4.0000

THERMODYNAMIC DATA
AR,AV,WAV,GAMMA=       0.83143D 04    0.60220D 27     7.270     1.540
RHO0,T0,EN0,C0,D=   0.7500D-02    2300.   0.62125D 24  0.2013D 04  0.2500D-09

FLOW AND GEOMETRY DATA
EM1,PS11,PS1F,PB1RD=     4.000   104.478    41.044     0.100
A0,RM1N,RSM1N,R0=     2.500    0.30374D-02    0.34812D-02    0.00000D 00
LAMDA0,LAMDA1,RMIN/LAMDA1,RSMIN/LAMDA1=    0.5797D-05    0.1281D-03    0.2372D 02    0.2718D 02

INTEGRATION DATA
DM0,NPHI,NR0,EPSEM=     0.100    10    10        0.100D-04
```

NX	NEM	XS	PH1MAX	QMAX	H / LDG	HF / LDG	H2 / LDG	DF / LDG	HE / LDG
1	47	0.0100	11.19	0.120D 25	0.824D 22/21.92	0.269D 07/ 6.43	0.777D 21/20.89	0.691D 06/ 5.84	0.653D 20/19.81
2	50	0.0178	12.15	0.121D 25	0.474D 22/21.68	0.162D 07/ 6.21	0.424D 21/20.63	0.418D 06/ 5.62	0.349D 20/19.54
3	54	0.0316	13.50	0.122D 25	0.237D 22/21.38	0.776D 06/ 5.89	0.196D 21/20.29	0.202D 06/ 5.30	0.154D 20/19.19
4	59	0.0562	15.27	0.123D 25	0.106D 22/21.02	0.295D 06/ 5.47	0.780D 20/19.89	0.770D 05/ 4.89	0.568D 19/18.75
5	64	0.1000	17.16	0.124D 25	0.421D 21/20.62	0.892D 05/ 4.95	0.268D 20/19.43	0.233D 05/ 4.37	0.175D 19/18.24
6	70	0.1778	19.55	0.124D 25	0.149D 21/20.17	0.219D 05/ 4.34	0.791D 19/18.90	0.575D 04/ 3.76	0.451D 18/17.65
7	77	0.3162	22.52	0.124D 25	0.471D 20/19.67	0.464D 04/ 3.67	0.203D 19/18.31	0.122D 04/ 3.09	0.100D 18/17.00
8	84	0.5623	25.65	0.124D 25	0.132D 20/19.12	0.901D 03/ 2.95	0.461D 18/17.66	0.237D 03/ 2.37	0.201D 17/16.30
9	92	1.0000	29.39	0.124D 25	0.335D 19/18.52	0.167D 03/ 2.22	0.959D 17/16.98	0.440D 02/ 1.64	0.381D 16/15.58
10	100	1.7783	33.26	0.124D 25	0.771D 18/17.89	0.305D 02/ 1.48	0 187D 17/16.27	0.801D 01/ 0.90	0.699D 15/14.84
11	108	3.1623	37.22	0.124D 25	0.165D 18/17.22	0.548D 01/ 0.74	0.353D 16/15.55	0.144D 01/ 0.16	0.126D 15/14.10
12	116	5.6234	41.19	0.124D 25	0.332D 17/16.52	0.981D 00/ 0.01	0.648D 15/14.81	0.258D 00/ 0.59	0.227D 14/13.36
13	124	10.0000	45.14	0.124D 25	0.641D 16/15.81	0.175D 00/ 0.76	0.117D 15/14.07	0.461D-01/ 1.34	0.405D 13/12.61

```
END RINGBD RUN


STATEMENTS EXECUTED= 1281233
```

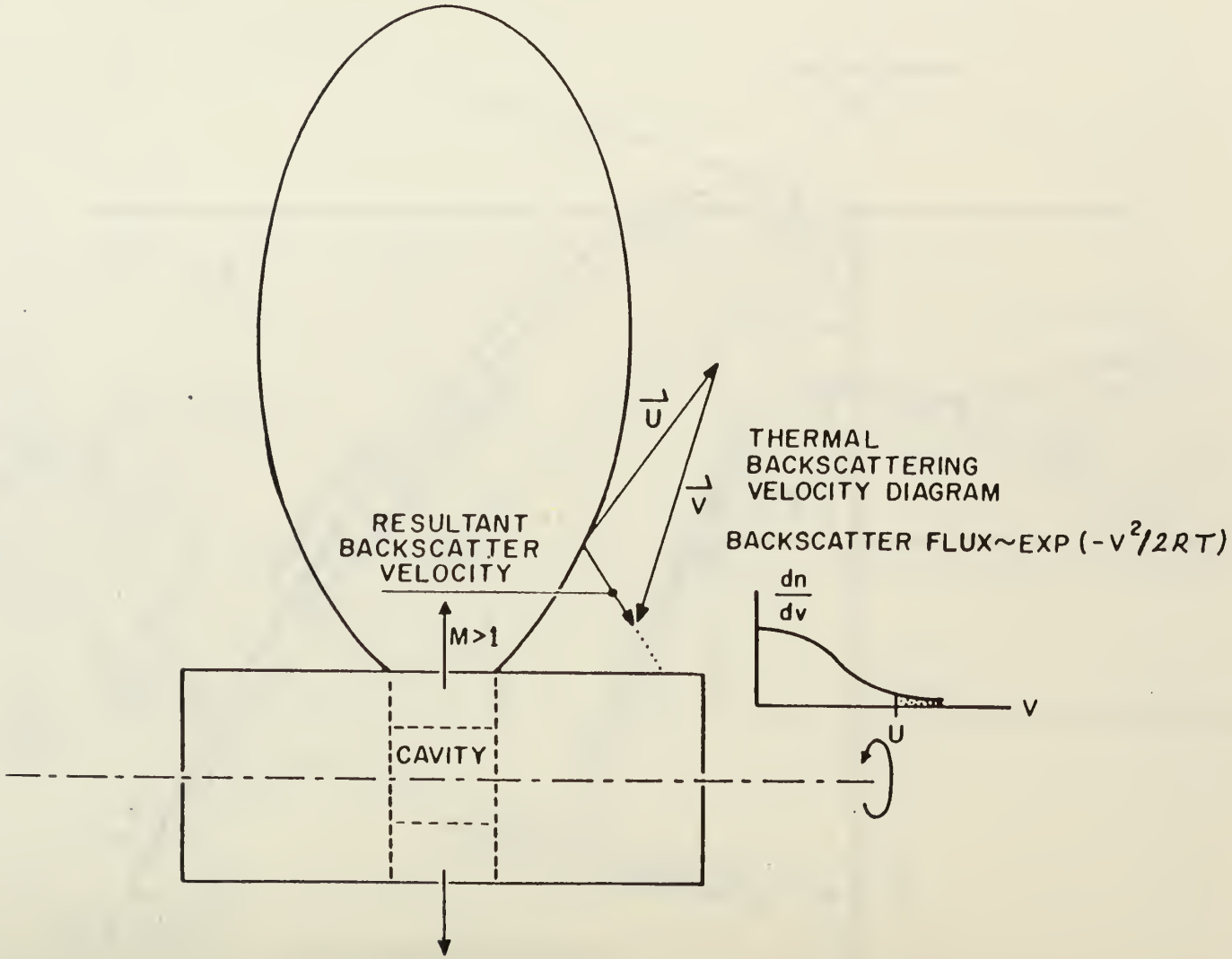

Figure 1. Thermal Backscattering from Laser Exhaust Plume

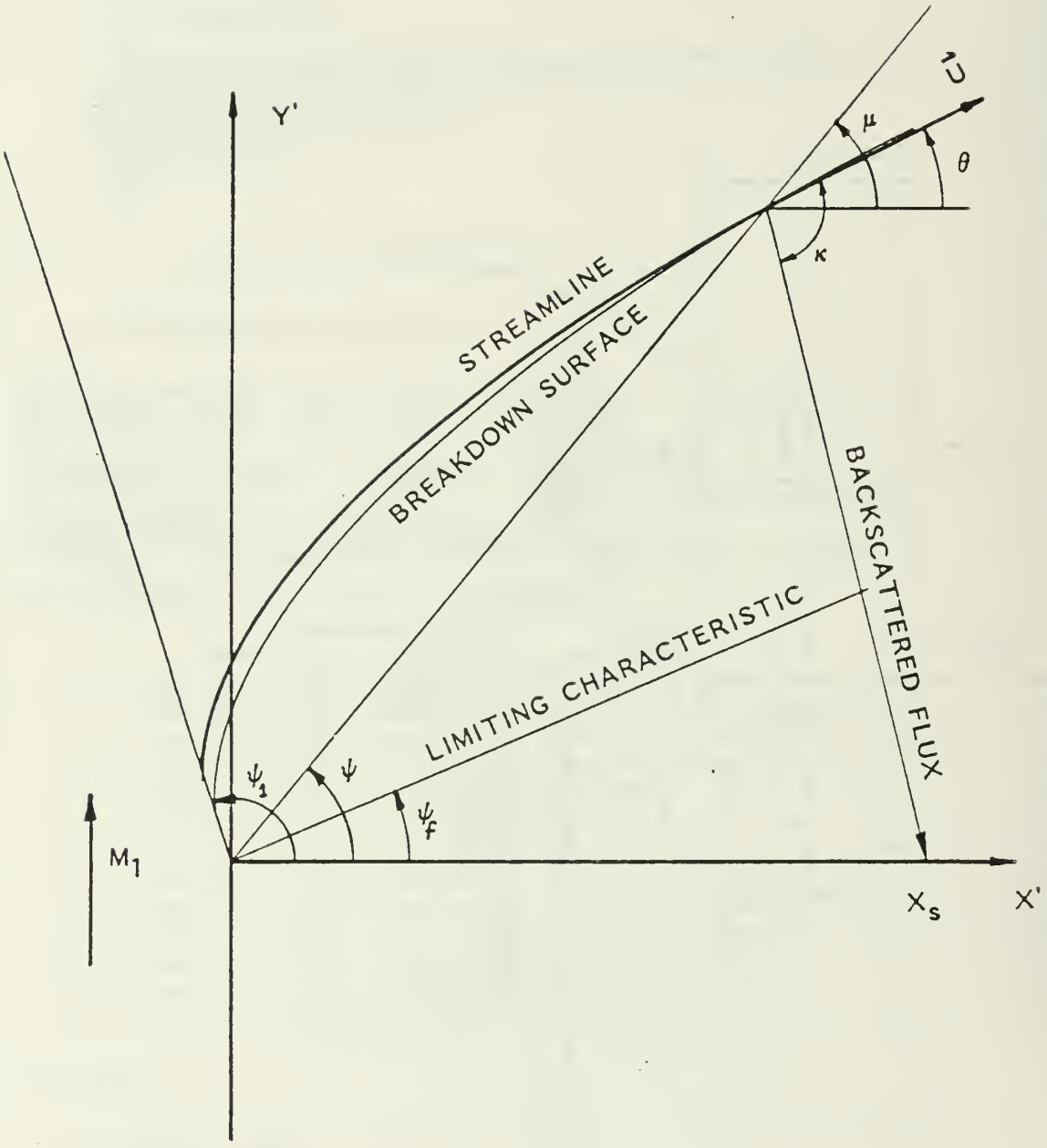

Figure 2. Prandtl-Meyer Centered Rarefaction Fan and Breakdown Surface (Schematic)

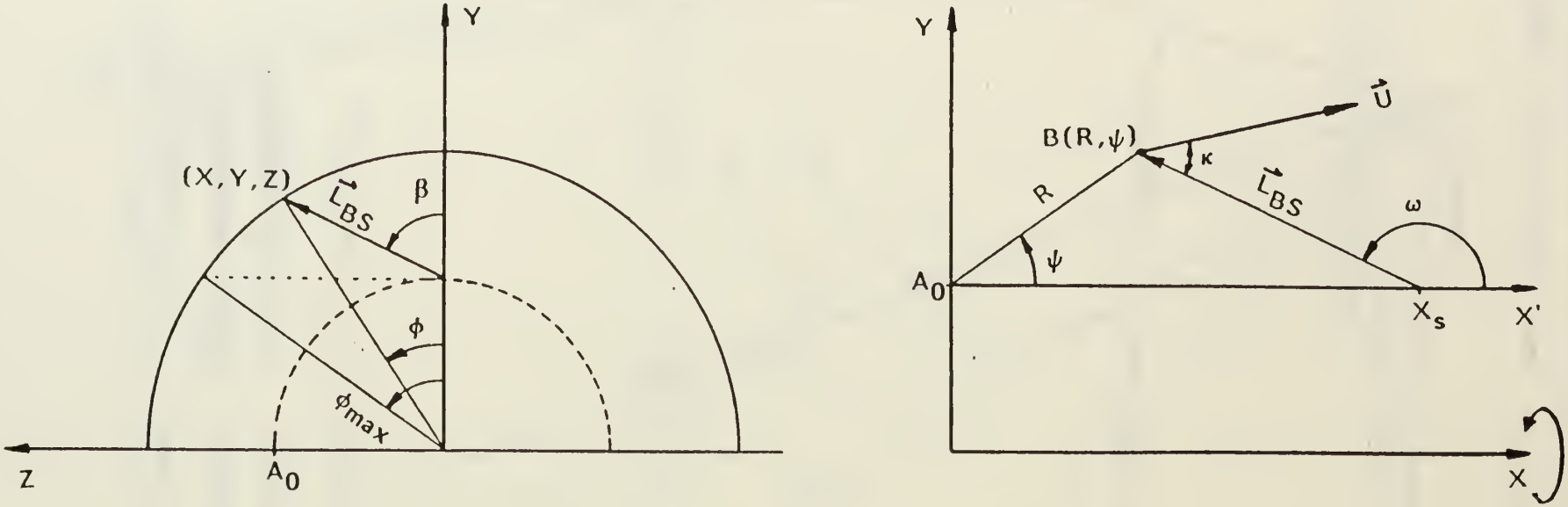

Figure 3. Flux Integration Scheme

B - Point on Breakdown Surface

(X,Y,Z) - Point on Breakdown Surface (Same point as B(R,ψ))

$\vec{L}_{BS}$ - Line of Sight

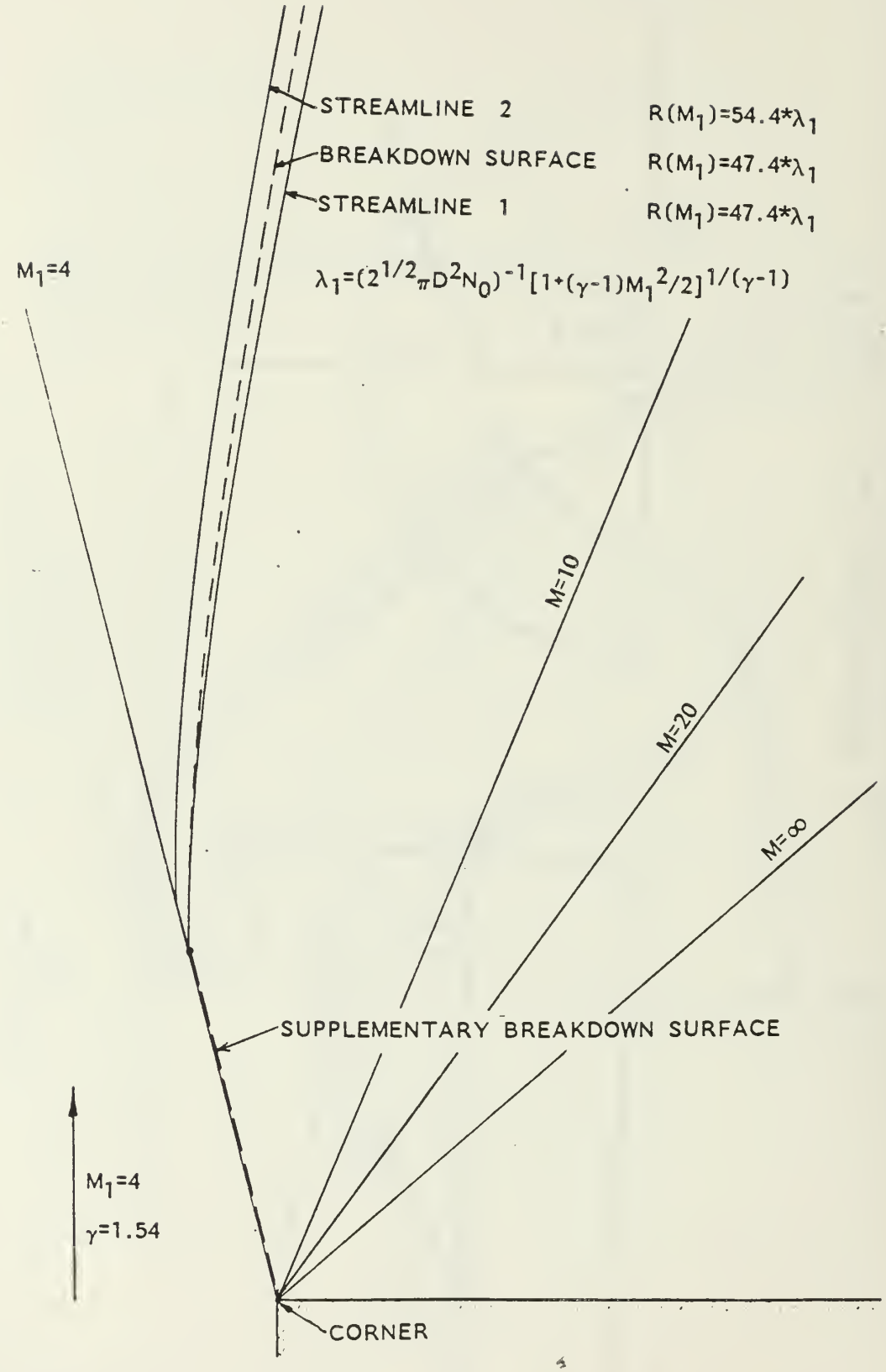

Figure 4. Prandtl-Meyer Flow Field Near the Corner, Including Actual Streamlines and Breakdown Surface

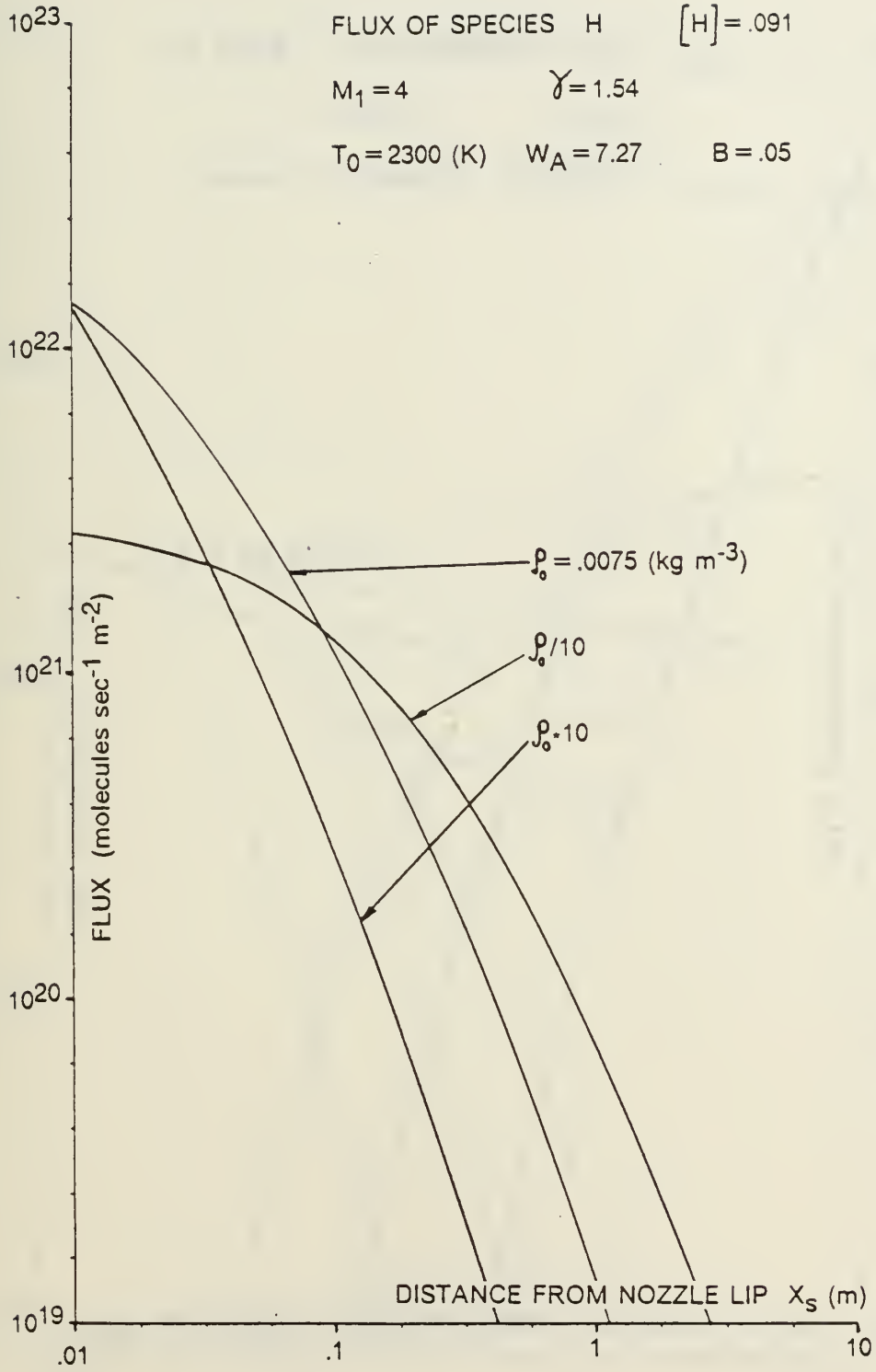

Figure 5. Flux of Species H at Various Stagnation Densities

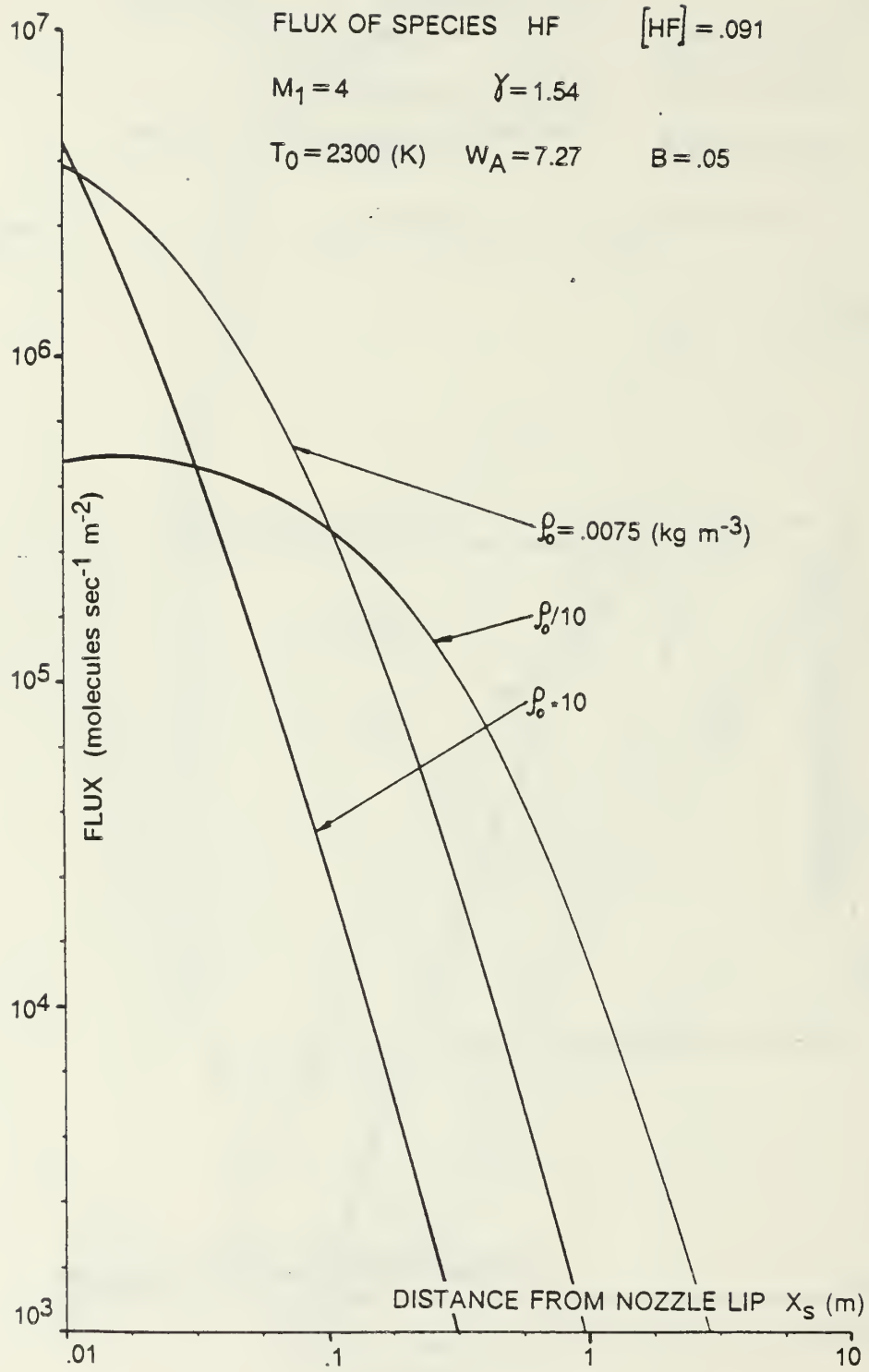

Figure 6. Flux of Species HF at Various Stagnation Densities

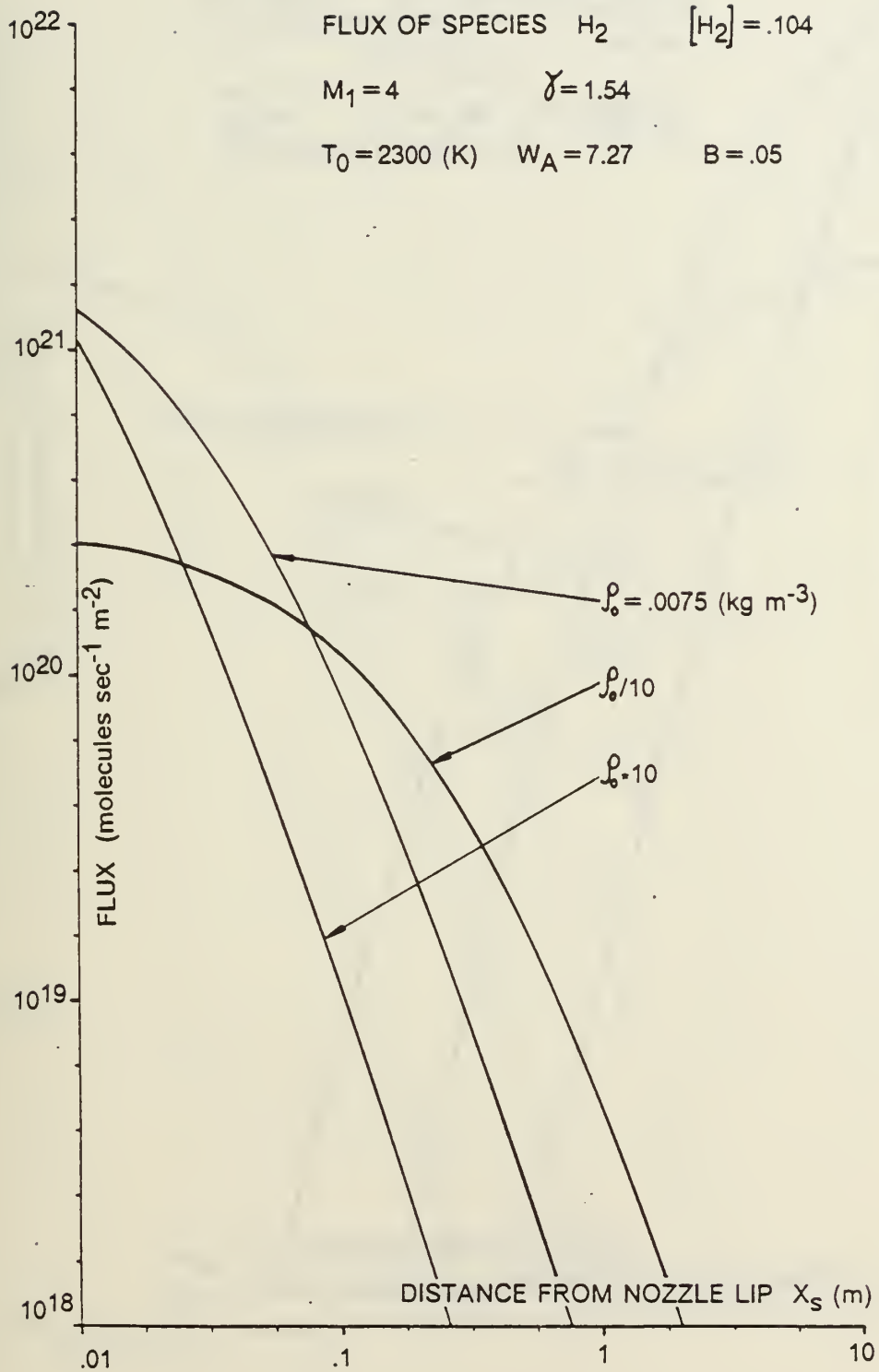

Figure 7. Flux of Species H_2 at Various Stagnation Densities

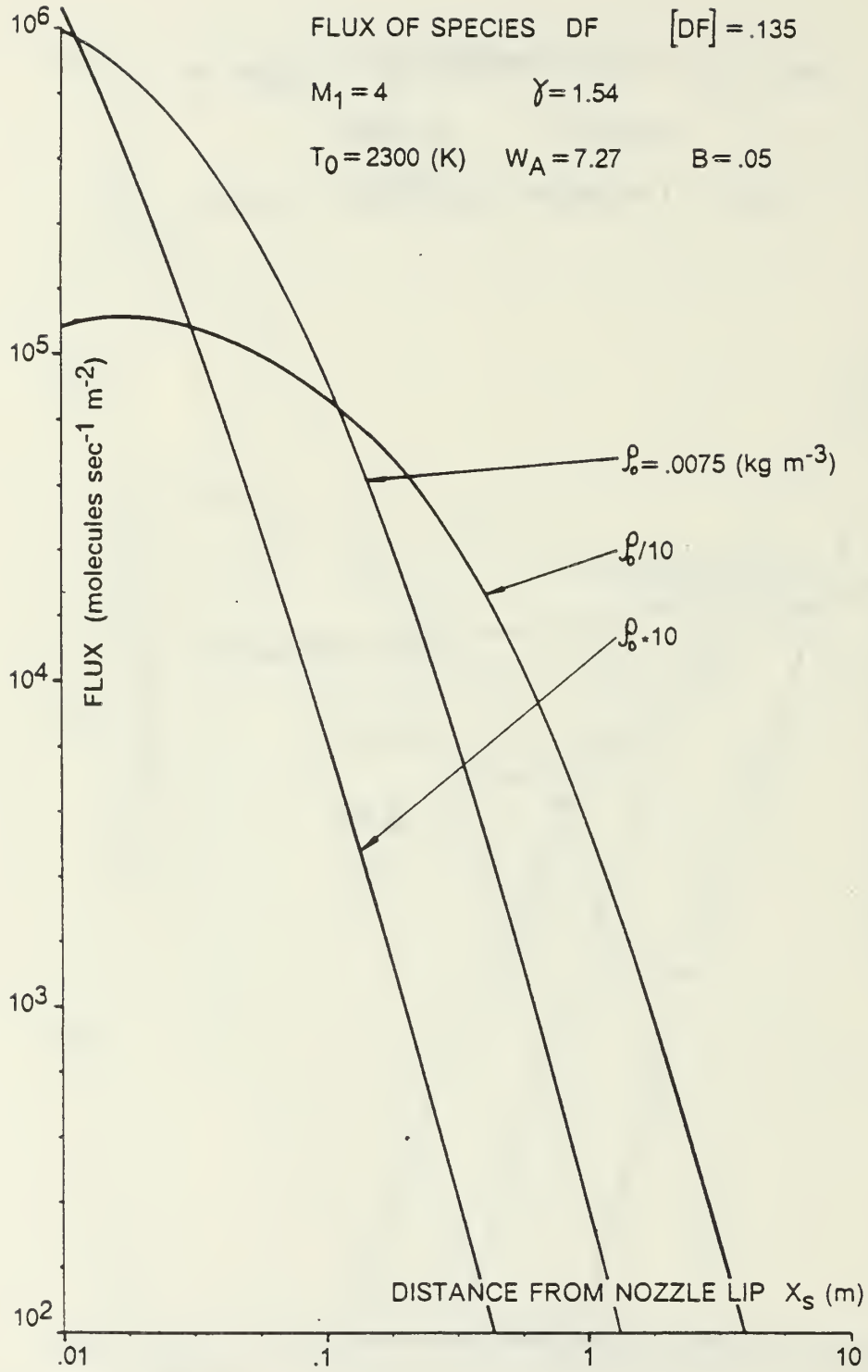

Figure 8. Flux of Species DF at Various Stagnation Densities

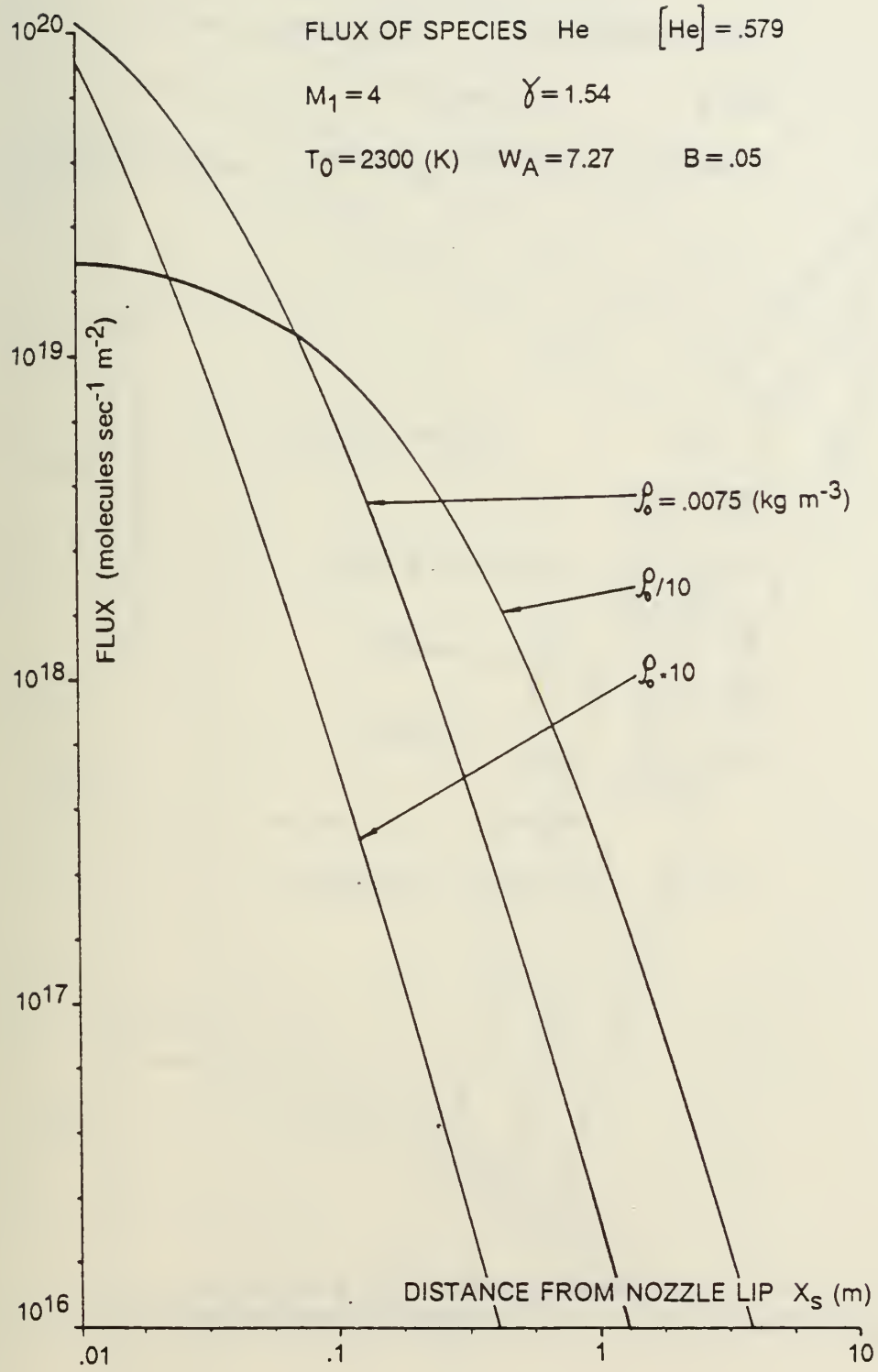

Figure 9. Flux of Species He at Various Stagnation Densities

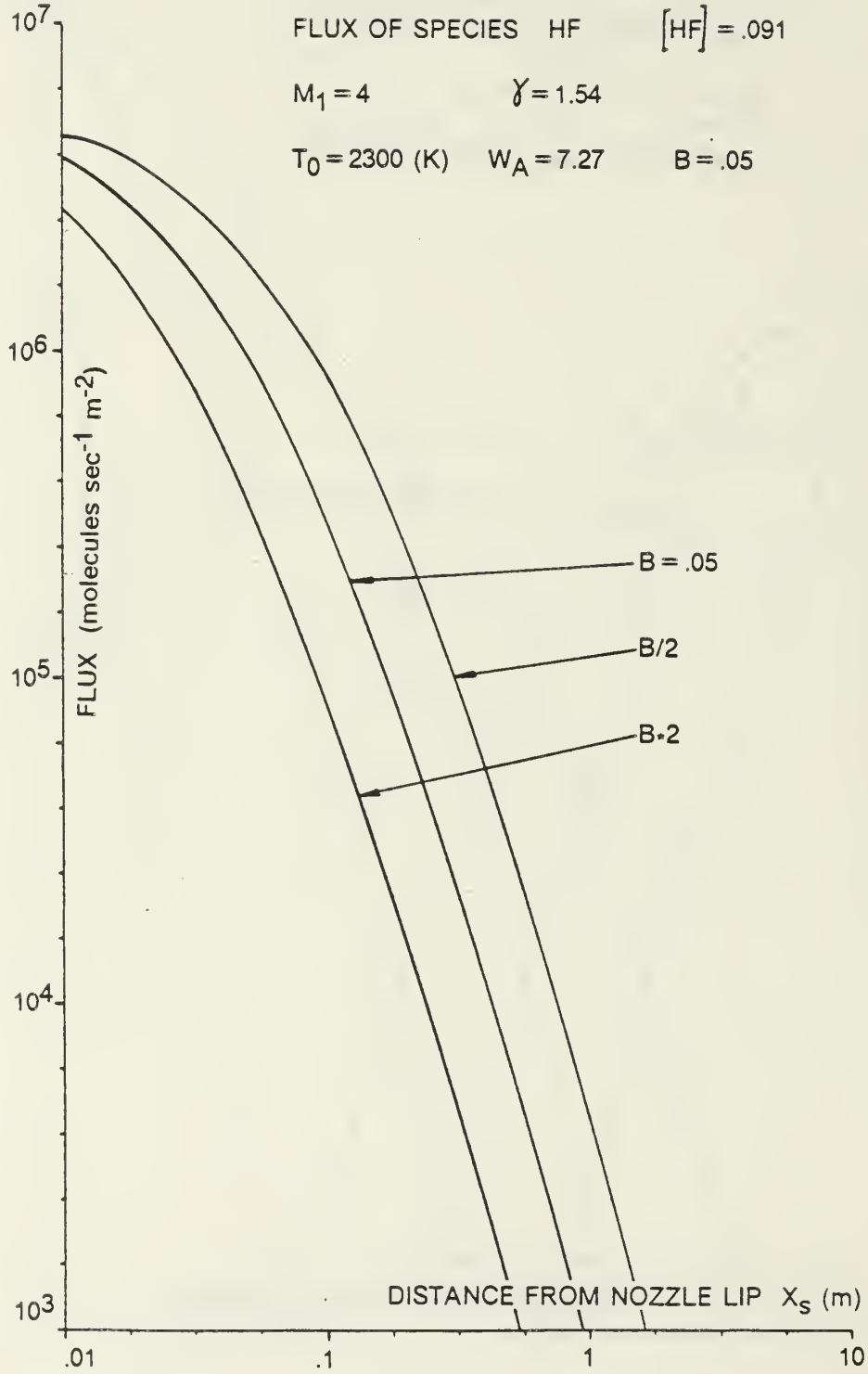

Figure 10. Flux of Species HF at Various Values of Breakdown Parameter

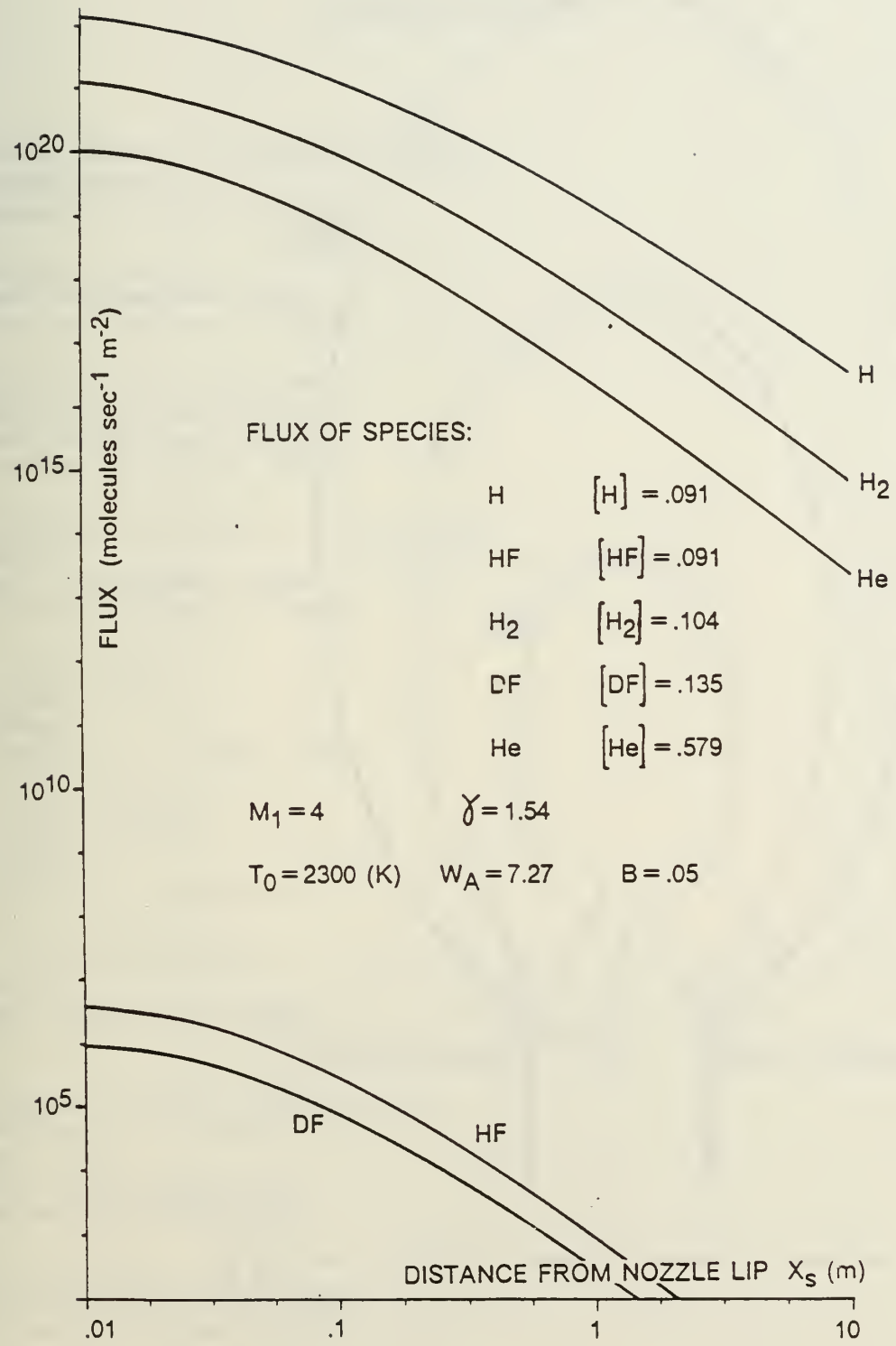

Figure 11. Flux of All Species at Typical Operating Conditions

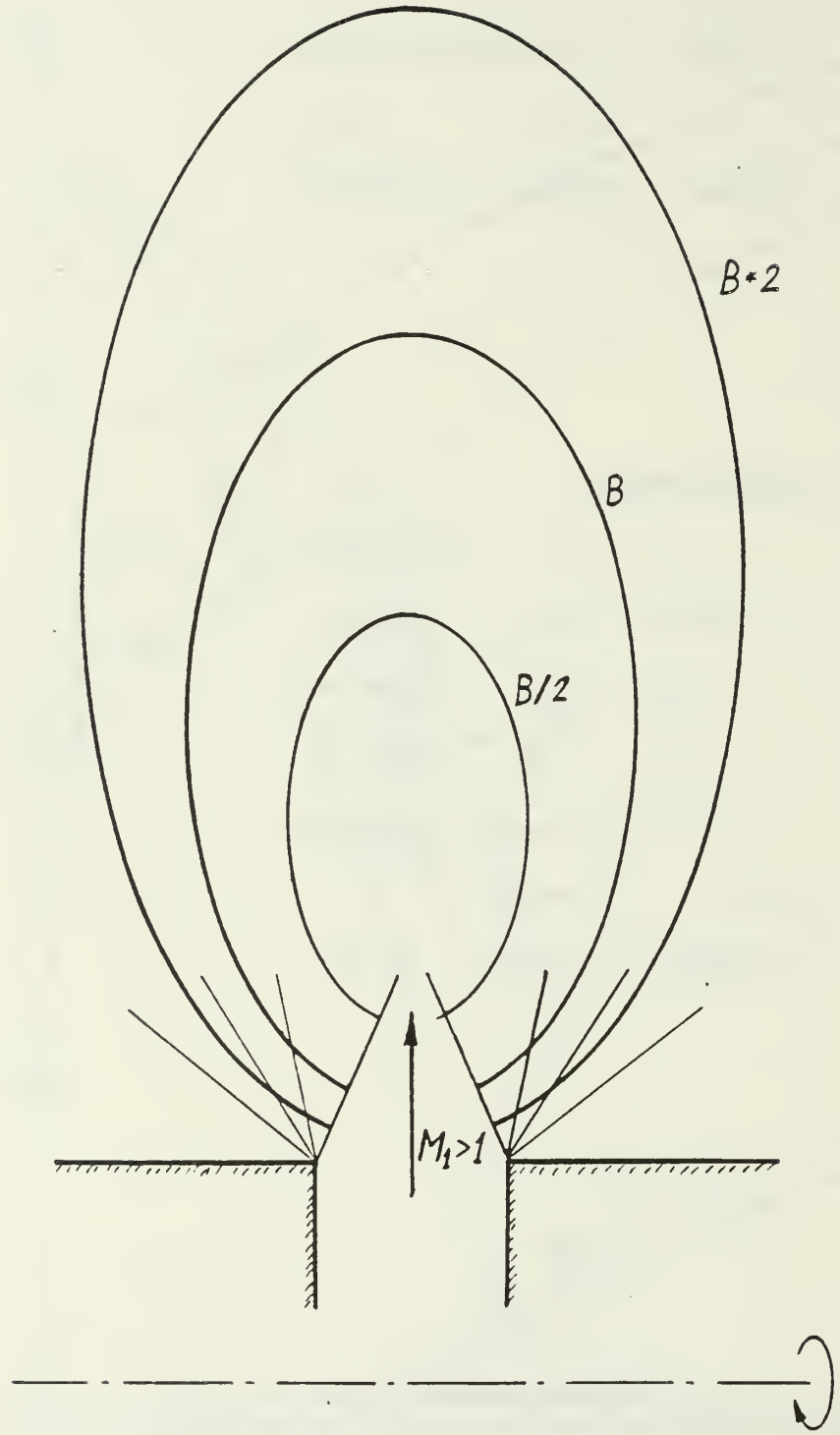

Figure 12. Schematic Display of Complete Breakdown Surface in a Ringjet Exhaust Plume

DISTRIBUTION LIST

		No. Copies
1.	Defense Technical Information Center Cameron Station Alexandria, Virginia 22314	2
2.	Library, Code 0142 Naval Postgraduate School Monterey, California 93943	2
3.	Department Chairman, Code 67 Department of Aeronautics Naval Postgraduate School Monterey, California 93943	1
4.	Distinguished Professor Allen E. Fuhs Code 72 Naval Postgraduate School Monterey, California 93943	4
5.	Mr. Neil Griff Pentagon SDIO/DEO Washington, DC 20301-7100	3
6.	Mr. Bruce Pierce Pentagon SDIO/DEO Washington, DC 20301-7100	1
7.	Dr. Joseph Falcovitz Code 72 Naval Postgraduate School Monterey, CA 93943-5100	8
8.	Associate Professor Oscar Biblarz Department of Aeronautics Code 67Bi Naval Postgraduate School Monterey, CA 93943-5100	1
9.	Dr. P. Avizonis Air Force Weapons Laboratory Kirtland Air Force Base, NM 87117	1
10.	Research Administration Office Code 012 Naval Postgraduate School Monterey, CA 93943-5100	1